iScience

CellPress
OPEN ACCESS

Article

Dimensionality reduction of complex dynamical systems

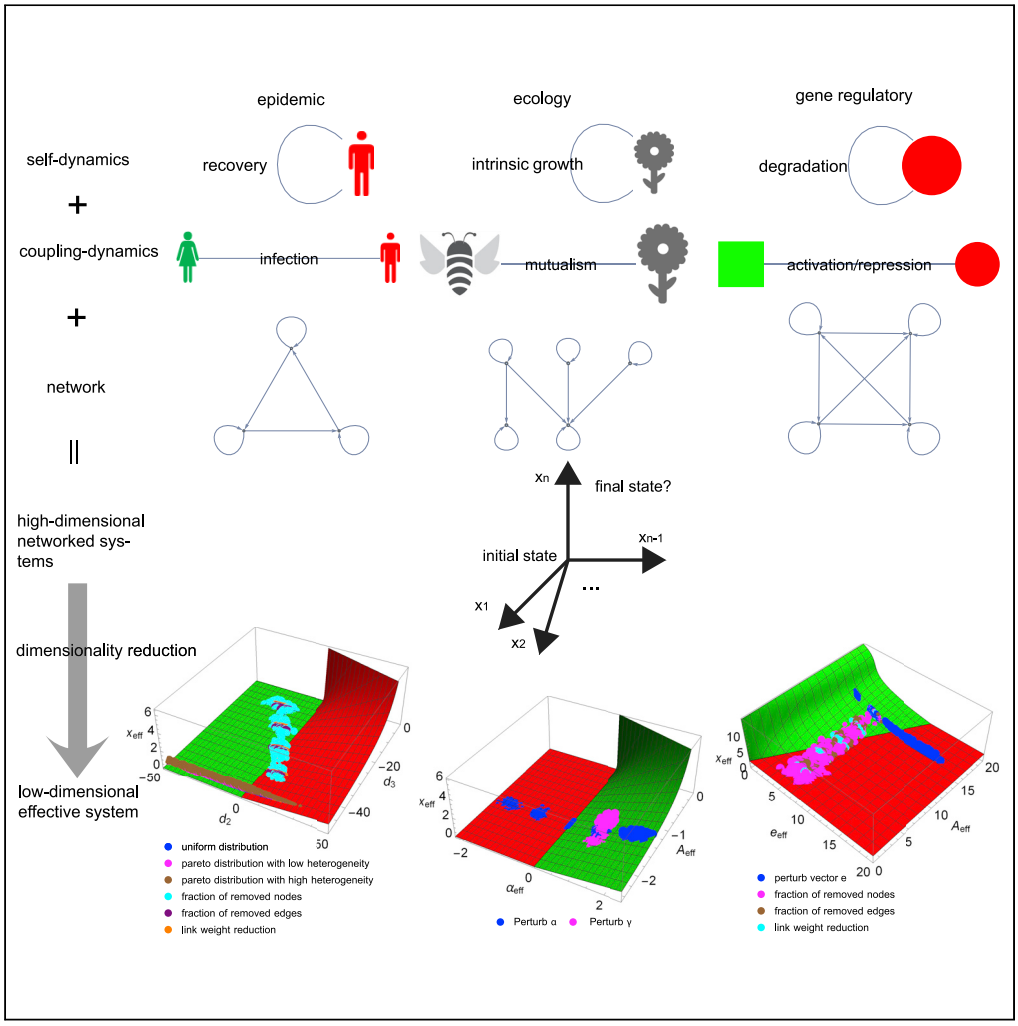

Chengyi Tu, Paolo D'Odorico, Samir Suweis

chengyitu@berkeley.edu, chengyitu@ynu.edu.cn

HIGHLIGHTS

We analytically collapse *N*-dimensional networked dynamics in low-dimensional manifolds

We test this approach on a variety of real-world complex problems

We accurately predict the system's response to changes in parameter values

We identify regions in parameter space corresponding to system's critical transitions

Tu et al., iScience *24*, 101912
January 22, 2021
https://doi.org/10.1016/j.isci.2020.101912

iScience

CellPress
OPEN ACCESS

Article

Dimensionality reduction of complex dynamical systems

Chengyi Tu,[1,2,3,5,*] Paolo D'Odorico,[3] and Samir Suweis[4]

SUMMARY

One of the outstanding problems in complexity science and engineering is the study of high-dimensional networked systems and of their susceptibility to transitions to undesired states as a result of changes in external drivers or in the structural properties. Because of the incredibly large number of parameters controlling the state of such complex systems and the heterogeneity of its components, the study of their dynamics is extremely difficult. Here we propose an analytical framework for collapsing complex N-dimensional networked systems into an S+1-dimensional manifold as a function of S effective control parameters with S << N. We test our approach on a variety of real-world complex problems showing how this new framework can approximate the system's response to changes and correctly identify the regions in the parameter space corresponding to the system's transitions. Our work offers an analytical method to evaluate optimal strategies in the design or management of networked systems.

INTRODUCTION

The study of complex dynamical systems is rapidly attracting interest within the multidisciplinary nonlinear science community, with cell biology, ecology, computer science, and meteorology being some of the many areas of investigation (Hughes et al., 2018; Gauthier et al., 2015; Ceballos et al., 2015; Johnson et al., 2017; Melbourne and Hastings, 2008; Oliver et al., 2015). Small perturbations due to management error, failure in one of the system's components, or environmental change (Woods, 2006; Walker et al., 2004; Rieger et al., 2009) take place at many different scales both in space and in time, leading to a broad range of impacts and even system collapse. To quantitatively investigate and understand these processes, we often need to understand their long-term behavior through an analysis of their stationary state(s), if any. The simplest kind of behavior is exhibited equilibrium points or fixed points. In general, a complex dynamical system may have multiple attractors of different types, depending on the parameter values, the initial conditions, and the structure of the interaction. In high-dimensional multivariate systems it is often impossible to characterize the extent of the domain of attraction of its stable equilibria and how the boundaries of such a domain change with different parameter values. Therefore, a crucial question in complexity science and dynamical system theory is identifying the factors that would prevent the state of the system from desired to undesired state shifts as a result of perturbations. Resilience is the ability of a system to adjust to perturbations while retaining its basic functionality, given by a specific functioning stable state (Arnoldi et al., 2016). Cell biology (Huang et al., 2005; Karlebach and Shamir, 2008), ecology (Allesina and Tang, 2012; Suweis et al., 2015b; Grilli et al., 2017), environmental science (Drever et al., 2006; Barlow et al., 2016), epidemic spreading (Pastor-Satorras et al., 2015; Boguna et al., 2013), and research in food security (Tu et al., 2019; Barthel and Isendahl, 2013; Suweis et al., 2015a) are just some of the many areas of research that are active in the investigation of mechanisms underlying systemic resilience. The probability that these systems will remain in a specific (e.g., functioning) state without shifting to alternative (undesired) attractors depends on the non-linear properties of the system's dynamics and on the intensity and type of perturbations they are exposed to. In the case of multidimensional complex systems, it is not possible to characterize the near equilibrium phase space as a function of the (many) parameters of the system.

Although great effort has been devoted to understanding the dynamical behavior and resilience of complex systems using one-dimensional methods (Lyapunov, 1992) (see Transparent methods, section Classic one-dimensional method to quantify resilience) and critical slowing down theory (Scheffer et al., 2009;

[1]School of Ecology and Environmental Science, Yunnan University, 650091, Kunming, China

[2]Yunnan Key Laboratory of Plant Reproductive Adaptation and Evolutionary Ecology, 650091, Kunming, China

[3]Department of Environmental Science, Policy, and Management, University of California, Berkeley, CA 94720-3114, USA

[4]Department of Physics and Astronomy "G. Galilei", University of Padova, 35131 Padova, Italy

[5]Lead contact

*Correspondence: chengyitu@berkeley.edu, chengyitu@ynu.edu.cn

https://doi.org/10.1016/j.isci.2020.101912

Scheffer et al., 2012; Suweis and D'Odorico, 2014) (see Transparent methods, section Critical slowing down), the study of the factors underlying the collapse of high-dimensional dynamical system remains an outstanding problem. At present, although there are well-developed theoretical frameworks to investigate the dynamical behavior and resilience of low-dimensional systems with few interacting components—especially in the traditional field of engineering control—significant challenges arise when these methods are applied to high-dimensional dynamical systems consisting of a large number of components that interact through a complex network. Recently, Gao et al.(Gao et al., 2016) developed a set of analytical tools with which it is possible to identify the natural control and state parameters of a high-dimensional networked system (where interactions are restricted on only positive) through mean-field approaches that reduce high-dimensional dynamics into an "effective" one-dimensional process that serves as a manifold for the average state of the system (see Transparent methods, section One-dimensional effective equation). In particular, the proposed framework allows for a systematic separation between the effects of system's dynamics and network's topology. The analytical results from these authors' analysis allow for the identification of the network's characteristics that can enhance or diminish the resilience of the stable states of the system. Furthermore, Laurence et al.(Laurence et al., 2019) developed a polynomial approximation to reduce complex networks based on spectral graph theory and showed that the proposed reduction of Gao et al.(Gao et al., 2016) is a special case of the general scheme when applied to uncorrelated random networks (see Transparent methods, section Dimension reduction based on spectral graph theory). This method has been just applied, for example, to interacting spreading dynamics in complex networks (Pan et al., 2020) and to predict the impact of network topology and dynamics on synchronization (Thibeault et al., 2020).

Unfortunately, these frameworks (Gao et al., 2016; Laurence et al., 2019) can be applied only to the particular case where the local dynamics at every node (hereafter termed "self-dynamics") as well as the pairwise dynamics (here called "coupling-dynamics") are expressed by functions that are not node specific but are the same at all nodes. In fact, only in such a case, the one-dimensional effective equation (Laurence et al., 2019; Gao et al., 2016; Tu et al., 2017) can be used to predict changes in resilience. Moreover, even when both self and coupling-dynamics are expressed by the same function at all nodes, the proposed framework works well only when the model parameters of the *N*-dimensional system are not too heterogeneous (e.g. have low coefficient of variation (CV)) (Tu et al., 2017). Unfortunately, such conditions, which are seldom found in natural and engineered complex systems, limit the real-world application of this framework. For example, in ecological community dynamics each species has a different growth rate (Holling, 1973); in an epidemic spreading, different groups typically have different infection or death susceptibilities (Pastor-Satorras et al., 2015); likewise, different chemical reactions commonly have different kinetics. Moreover, in some cases we may want to model different network nodes with different functions (Harush and Barzel, 2017; Hens et al., 2019); for example, some genes may be regulated by Michaelis-Menten type of interactions, whereas other can be involved in both regulation and chemical binding coupling. Therefore, a more general framework to explore the functioning or the collapse of networked systems with node-specific self-dynamics and coupling-dynamics is needed to fill the gap existing between theory and real-world problems.

Here we develop a general analytical framework that can be used to reduce the dimensionality of the "order" parameter space as a function of a set of effective "control" parameters, defined as those parameters that drive the functioning (associated to specific system states) and the resilience of any networked system, including those with node-specific self-dynamics and coupling-dynamics. Specifically, our framework generalizes the one-dimensional effective equations introduced by Gao and collaborators (Gao et al., 2016) in two respects: (1) we can reduce the starting N-dimensional dynamics in an effective equations of one *or more* dimension, depending on the desired degree of accuracy and heterogeneity of model parameters; (2) we can provide a dimensionality reduction not only for the case where all nodes interact through the same mechanisms (functional form) while having diverse parameters but also for non-homogeneous dynamics mechanisms whereby the functional form of self-dynamics and coupling-dynamics differ across nodes.

As we will show, the proposed framework relies on the use Hadamard product approximation and Chebyshev's polynomial decomposition to reduce non-linear functions into polynomial form. Analogous to the classic method used for one-dimensional dynamics (Lyapunov, 1992; Laurence et al., 2019; Gao et al., 2016), our approach allows us to investigate the possible occurrence of transitions (broadly defined) from a functioning stable state to an undesired one where the networked system collapses or stops functioning in the desired way. Therefore, we can predict collapse induced by changes in both the interaction

network (e.g. its connectivity) as well as the self-dynamics and coupling-dynamics (e.g. growth rates) from node to node. In summary, we show how the average dynamics of a high-dimensional networked system can be captured by a low-dimensional manifold characterizing the role of interaction network, self-dynamics, and coupling-dynamics in the equilibrium states of the system and their dependence on the system's parameters. The analytical expression for this manifold allows us to predict transitions in the underlying nonlinear dynamics as a function of few, key order parameters.

RESULTS

Dimensionality reduction and resilience

Consider a networked system consisting of N nodes whose states $\mathbf{x} = (x_1, \ldots, x_N)^T$ follow the dynamic equation

$$\frac{dx_i}{dt} = F_i(x_i) + \sum_j^N A_{ij} G_i(x_i, x_j) \qquad \text{(Equation 1)}$$

where $F_i(x_i)$ is the "local" dynamics at node i (or "self-dynamics") and $G_i(x_i, x_j)$ is the dynamics expressing the coupling of node i with its neighbors j (or "coupling-dynamics"), according to the adjacency matrix $\mathbf{A} \in R^{N\times N}$, representing the interaction network of the system, with A_{ij} capturing the interaction $i \leftarrow j$. Resilience loss can be induced by changes in any of the parameters of the network $\mathbf{A}$, of the self-dynamics $F_i(x_i)$, or of the coupling-dynamics $G_i(x_i, x_j)$. Recently, Gao et al.(Gao et al., 2016) investigated the resilience of this system in the particular case in which the functions F and G expressing the self-dynamics and coupling-dynamics are the same at all nodes, i.e., $\forall i, F_i(x_i) = F(x_i)$ and $\forall i, G_i(x_i, x_j) = G(x_i, x_j)$. Thus, these authors developed a method to explore the resilience of a node-uniform complex interacting system (i.e., Equation (1) with F and G independent of i). To date, a framework to investigate the networked dynamics (1) with node-specific self-dynamics and coupling-dynamics is still missing. To formulate a more general framework for the analysis of the resilience for a networked system, we first define the mean field operator (Gao et al., 2016) $\mathcal{L}(\mathbf{x}) = \frac{1}{N}\sum_{j=1}^N s_j^{out} x_j / \frac{1}{N}\sum_{j=1}^N s_j^{out} = \frac{\langle \mathbf{s}^{out} \cdot \mathbf{x} \rangle}{\langle \mathbf{s}^{out} \rangle}$ where $\mathbf{s}^{out} = (s_1^{out}, \ldots, s_N^{out})$ is the vector of the out-degree of matrix $\mathbf{A}$; then, we characterize the effective state of the networked system using the weighted average node state $x_{eff} = \mathcal{L}(\mathbf{x})$. If the network's degree correlation is low, we can assume that the Hadamard product approximation holds (see Transparent methods, section Validation of the Hadamard product). Then, applying Chebyshev expansion to approximate $F_i(x_i)$ and $G_i(x_i, x_j)$ with polynomial functions of order m and n, respectively, Equation (1) can be reduced to

$$I(d_1, \ldots, d_S, x_{eff}) = \frac{dx_{eff}}{dt} \approx \sum_{s=1}^{S} d_s * x_{eff}^{s-1} \qquad \text{(Equation 2)}$$

where $S = \max(m,n)$, $d_s = \begin{cases} B_{eff}^s + A_{eff} * C_{eff}^s, s \in [1, \min(m,n)] \\ A_{eff} C_{eff}^s, s \in [m+1, n], m<n \\ B_{eff}^s, s \in [n+1, m], n<m \end{cases}$; $A_{eff} = \mathcal{L}(\mathbf{s}^{in})$, $B_{eff}^s = \mathcal{L}(B^s)$, and $C_{eff}^s = \mathcal{L}(C^s)$.

$B^k = (b_{1,k}, \ldots, b_{N,k})^T$ is the column of the k-th term of the m-order Chebyshev polynomials (Boyd, 2001; Mason and Handscomb, 2002) (see Transparent methods, section Self-dynamics and coupling-dynamics are polynomials) approximating the self-dynamics $F_i(x_i)$, and $C^l = (c_{1,l}, \ldots, c_{N,l})^T$ is the column of the l-th factor of the n-order Chebyshev polynomials approximating the coupling-dynamics $G_i(x_i, x_j)$ (see Transparent methods, section Reduce high-dimensional equations). Therefore, we map the dynamics of Equation (1) into Equation (2) and study the resilience of the system, through the behavior of x_{eff} at steady state and its response to a perturbation of one or more of these S parameters. In particular, the conditions for stability of a state x_{eff}^* of the dynamics can thus be associated with a region expressed by the equation set:

$$\begin{cases} I(d_1, \ldots, d_S, x_{eff}^*) = 0 \\ \dfrac{dI}{dx_{eff}} < 0 \end{cases} \qquad \text{(Equation 3)}$$

where the function I represents the system's dynamics and $d_1, \ldots, d_S$ are their control parameters.

Equation (3) allows us to take advantage of theoretical tools developed for one-dimensional systems (see Transparent methods, section Classic one-dimensional method to quantify resilience). In fact, regardless of the microscopic details of any perturbation acting on the system, the way such a perturbation impacts the

state of the networked system is fully accounted for by the corresponding changes in the control parameters $(d_1, d_2, \ldots, d_S)$ of the effective dynamics. This implies that the rather complex and unpredictable behaviors of networked systems can be captured by a low-dimensional space given by $I(d_1, \ldots, d_s, x^*_{eff})$ that serves as a manifold for the complex networked dynamics near their stationary state. The structure of this manifold is uniquely determined by the polynomial of the effective equation.

In addition, in order to measure the projection distance from the point $(d_1, \ldots, d_S, x^*_{eff})$ obtained from Equation (1) and the stationary solution of the low-dimensional resilience function $x(d_1, \ldots, d_S)$ obtained from Equation (3), we define the following function, which allows us to estimate the error of the proposed approximation $err_x = |x_{eff} - x(d_1, \ldots, d_S)|$. If this error distance is small, the point of numerical simulation is near the surface of low-dimensional resilience function, which means that this framework works well.

Application to real-world examples

In many networked systems of practical importance, we can use the above theoretical approach to relate high-dimensional network dynamics to low-dimensional phase space manifolds and investigate analytically the system's behavior as a function of its order parameters. We adopt a set of widely used dynamical models along with experimental static networks and extensive numerical simulations to test the predictions of our framework. In particular, we also investigate a case poorly studied in the literature, where coupling-dynamics varies among different nodes.

Quantifying effectiveness of mitigation measures in epidemic dynamics

We first consider a system of N individuals with some of them infected by a virus or other transmissible disease that spreads through the system as individuals interact. In these dynamics, it is often important to understand the effectiveness of various measures (such as social distancing or quarantining) in limiting the spread of the epidemic. We consider the dynamics of a commonly used susceptible-infected-susceptible (SIS) model (Pastor-Satorras et al., 2015; Boguna et al., 2013), governed by the equation

$$\frac{dx_i}{dt} = -e_i x_i + \sum_j^N A_{ij}(1 - x_i)x_j \qquad \text{(Equation 4)}$$

where $0 \leq x_i \leq 1$ denotes the probability that node i is in the infected state, e_i is the recovery rate of node i, and A_{ij} represents the infection rate of node i as a result of the interaction with node j. The first term on the right-hand side of Equation (4) accounts for the process of recovery, and the second term accounts for the process of infection. We notice that in this case we account for the heterogeneity of the system because each individual has its own recovery rate and interactions with other individuals according to the network, $\mathbf{A}$. Considering the case of parameter values (i.e., $\mathbf{e}$ and $\mathbf{A}$) for which the steady state of the system is positive (i.e., $\mathbf{x}*(t \to \infty) > 0$ or "epidemic active phase"), we can investigate how such a stationary state changes as a result of mitigation measures such as drug development (and consequent increase in the recovery rates), quarantine of individuals (i.e., node removal), social distancing, or use of personal protection to decrease the probability of infection (i.e., removal or weakening of interactions, respectively). What measures are the most effective in making the system collapse and undergo a transition to $\mathbf{x}* = 0$? We now apply our framework to address this question. The effective equation of the SIS model is $\frac{dx_{eff}}{dt} = d_2 x^1_{eff} + d_3 x^2_{eff}$ where $d_2 = B^2_{eff} + A_{eff} = -e_{eff} + A_{eff} = \mathcal{L}(-\mathbf{e}) + \mathcal{L}(\mathbf{s}^{in})$, $d_3 = -A_{eff} = -\mathcal{L}(\mathbf{s}^{in})$. It is easy to see from this one-dimensional equation that the dynamics have two steady states: $x^*_{eff} = -d_2/d_3$ and $x^*_{eff} = 0$. In other words, our framework predicts that the steady states of this high-dimensional Equation (4) are two surfaces, $x^*_{eff} = -d_2/d_3$ and $x^*_{eff} = 0$ in the space (x_{eff}, d_2, d_3), and their stability depends on the order parameters d_2 and d_3.

We test these predictions by simulating the dynamics and exploring the effect of changes in the parameters characterizing the self-dynamics and network interactions. As empirical network for the SIS model, we use the real contact dataset from the 2009 ACM Hypertext conference where the SocioPatterns project deployed the Live Social Semantics application (Isella et al., 2011; Rossi and Ahmed, 2015). This empirical network has 113 nodes and 2,196 edges. We express the recovery rates $\mathbf{e} = (e_1, \ldots, e_N)^T$ as random parameters drawn from a uniform distribution between 0 and $2\mu_e$ where μ_e is thus the mean recovery rate and default value $\mu_e = 30$. We set two initial conditions for $\mathbf{x}(t = 0)$: a low contagion initial state whose elements are drawn from a uniform distribution between 0 and 0.1, and a high contagion initial state whose elements are drawn from a uniform

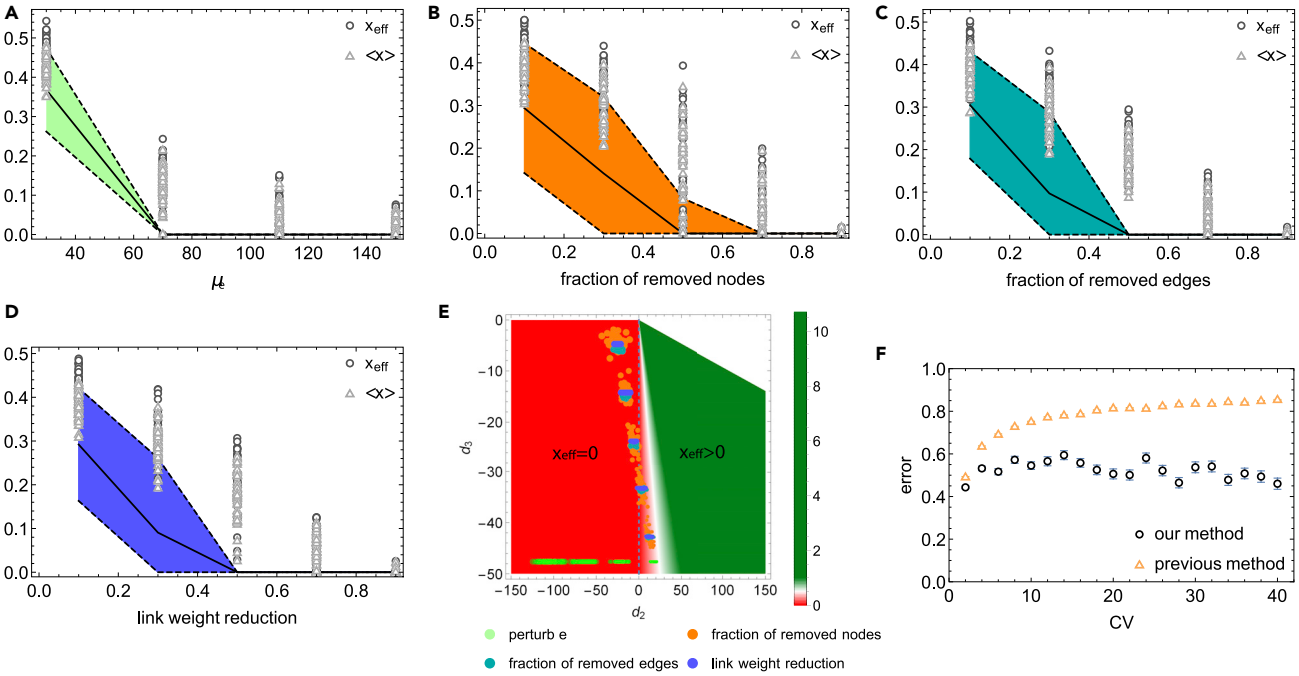

Figure 1. Results obtained from numerical simulation and theoretical predication as a function of changes on epidemic dynamics

The solution of the epidemic dynamics given by Equation (4) as a function of changes in (A) the mean μ_e of vector **e** drawn from a uniform distribution (and with fixed contact network A).

(B) The fraction of randomly removed nodes ranging between 0 and 0.8.

(C) The fraction of randomly removed edges ranging between 0 and 0.8.

(D) The links weight $a_{ij}' = a_{ij} * (1 - r)$ with reduction parameter r ranging from 0 to 0.8 and where the vector **e** is drawn from a uniform distribution between 0 and $2\mu_e$ (andμ_e = 30). In each panel, the solid black line is obtained by averaging the analytical prediction $<x^*_{eff}(d_2, d_3)>$ over 50 realizations of matrix **A** and vector **e** through $d_2(e_{eff}, A_{eff})$ and $d_3(A_{eff})$. The dashed line represents the corresponding confidence level of three standard deviations.

(E) The density plot is given by the analytical form of x_{eff} as a function of d_2, d_3, whereas colored points shown on the varied perturbations collapse onto the manifold. For each perturbation type, the points size scales with the magnitude of the perturbation.

(F) Error comparison between our method and the previous method by Gao et al. (2016) as a function of the coefficient of variation, CV, of the vector, **e**, drawn from lognormal distribution with the mean 50.

distribution between 0.9 and 1. The presented results are averaged over both low and high contagion initial condition, as initial conditions do not play any role in this case (see Transparent methods).

Figures 1A–1D show the results for $<x> = \sum_{i=1}^{N} x_i/N$ and $x_{eff} = \frac{\langle \mathbf{s}^{out} \mathbf{x} \rangle}{\langle \mathbf{s}^{out} \rangle}$ obtained from numerical simulation of Equation (4) as a function of the following changes in the model's parameters: (1) we increase the average recovery rate (μ_e) to investigate the effect of increasingly effective treatment therapies; (2) we increase the number of individuals in quarantine (by randomly removing an increasing fraction of network nodes); (3) we intensify the effectiveness of social distancing measures (removing randomly an increasing fraction of network edges); and (4) we intensify the effectiveness of personal protection equipment (decreasing the contact network weights). We find that the results from the numerical simulations collapse onto the manifold $x^*_{eff}(d_2, d_3)$ (Figure 1E) with relatively small error. To better appreciate the approximation errors, in Figures 1A–1D we also show the analytical solution $x^*_{eff}(d_2, d_3)$. We highlight that $d_2(e_{eff}, A_{eff})$ and $d_3(A_{eff})$ depend on the specific realization (of matrix A and vector $\boldsymbol{\alpha}$) and thus the black continuous lines represent the average $<x^*_{eff}(d_2, d_3)>$ (with colored area representing the three standard deviations) over the different realizations. In addition, we compare the errors of our approximation with respect to those obtained by Gao et al. (Gao et al., 2016), varying the heterogeneity of the networks parameters as measured by the coefficient of variation (CV). We find, as expected, that for small CV the two methods behave similarly, whereas for intermediate and large CV, our approach gives a better approximation (Figure 1F).

We can thus see that small changes in d_2 may lead to the collapse of the epidemic, i.e., a transition from $x_{eff}>0$ to $x_{eff} = 0$. Specifically, if $A_{eff}>e_{eff}$ then $d_2>0$ and $x_{eff}>0$. Vice versa, if $A_{eff}<e_{eff}$ then $d_2< 0$ and

$x_{eff} = 0$. As the recovery rate μ_e increases, d_2 decreases, thereby leading to a decrease of x_{eff} to zero. Similarly, as mutual interactions are reduced (e.g., node or edge removal or reduction in the network's weights), A_{eff} decreases, leading to a decrease in d_2, d_3, thereby driving x_{eff} toward the collapse. We highlight that the presented results are independent of the system's initial conditions and our framework works for different distribution even with high heterogeneity (see Transparent method, section Heterogeneous networks). We note that, even in this simple example, where the system dynamics are already expressed in polynomial form and therefore there is no need for the Chebyshev approximation, our framework goes beyond the classic mean field approximation (Pastor-Satorras et al., 2015) or the one dimensional effective equation previously proposed (Gao et al., 2016). In fact, here we are able to consider individual recovery rates and heterogeneity in the weights of the contact network (Tu et al., 2019). As expected, in the limit $e_i = \mu_e$, $\forall i$ and constant weights for all contacts, our results converge to those from previously studied approximation methods.

Effect of perturbations on multidimensional generalized Lotka-Volterra dynamics

Another suitable application of our framework can be found in population dynamics for interacting ecological species and the understanding of the interplay between species interaction networks and biodiversity (Suweis et al., 2013, 2015b; Dakos and Bascompte, 2014; Cenci et al., 2017; Grilli et al., 2017). The generalized Lotka-Volterra (GLV) dynamics are a set of first-order, non-linear, differential equations frequently used to describe the population dynamics of interacting species in community ecology. Species interaction network can be used to model competition, predator-prey, and mutualistic relationships among an arbitrary number of species. The GLV dynamics for species i are given by

$$\frac{dx_i}{dt} = \alpha_i x_i + \sum_{j=1}^{N} x_i A_{ij} x_j \qquad \text{(Equation 5)}$$

where N is the number of species in the community, $x_i \geq 0$ is the population size of species i, α_i is its intrinsic growth rate, and A_{ij} is the interaction between species i and j. The effective equation of the model is $\frac{dx_{eff}}{dt} = d_2 x^1_{eff} + d_3 x^2_{eff}$ where $d_2 = \alpha_{eff} = \mathcal{L}(\boldsymbol{\alpha})$, $d_3 = A_{eff} = \mathcal{L}(\mathbf{s}^{in})$. Thus, the effective equation shows that for a given set of parameters the dynamics have only one stable equilibrium, as confirmed by the global equilibrium analysis of Equation (5) with the Lyapunov function (Serván et al., 2018). We use our framework to identify the changes in the parameter space that are associated with a collapse from a state of species coexistence (i.e., $x_{eff} > 0$), to the state where all species go extinct ($x_{eff} = 0$).

For instance, we consider the case of a community composed of N species comprising N_p plants and N_a animals such as insects serving as pollinators with $N = N_p + N_a$. x_i^p and x_j^a denote the abundances of the i-th plant species and the j-th animal pollinator species, respectively, and $\mathbf{x} = \{x_1^p, x_2^p, \ldots, x_{N_p}^p, x_{N_p+1}^a, \ldots, x_N^a\}$ is a vector expressing the population size of each of the species in the community. Species-specific intrinsic growth rates are the elements of the N-dimensional vector $\boldsymbol{\alpha}$. The species' interaction matrix A is composed by four blocks, two of which describe the direct competitive interactions among plants (Ω_{pp}) and insects (Ω_{aa}), respectively and the other two define the mutualistic interactions between insects and plants (Γ_{pa}) and vice-versa (Γ_{ap}). Therefore, the interaction matrix A has the following structure $A = \begin{bmatrix} \Omega_{pp} & \Gamma_{pa} \\ \Gamma_{ap} & \Omega_{aa} \end{bmatrix}$. Following previous studies (Dakos and Bascompte, 2014), for each plant and animal species we set competition coefficients β (in the Ω_{pp} and Ω_{aa} matrices) sampled from a uniform distribution with maximum -0.001 and mean $-1/n^{p,a}$, where n^p, n^a are the number of plant or animal species, respectively. In other words, the interaction matrix A_{ij} exhibits a mixture of positive and negative signs and also correlation among elements and where intraspecific competition coefficient is set equal to -1. Γ_{pa} and Γ_{ap} matrices describe how species are mutualistically interacting. We expressed the weights of this interaction matrix using a trade-off function that defines the mutualistic dependence between species j and i as a function of their degree: $\gamma_{ij} = \gamma y_{ij}/k_i$, where γ is drawn from a normal distribution with mean μ_γ and standard deviation $\sigma_\gamma = |\mu_\gamma/3|$, k_i is the degree of species i, and $y_{ij} = 1$ if species i and j interact and zero otherwise (Dakos and Bascompte, 2014). The adjacency matrix $\mathbf{Y}$ is taken directly from empirical network of a hummingbird community in a highland temperate forest in central Mexico (Lara, 2006). We then set $\boldsymbol{\alpha} = (\alpha_1, \ldots, \alpha_N)^T$ as a vector whose elements are drawn from a normal distribution with mean μ_α and standard deviation $\sigma_\alpha = |\mu_\alpha/3|$. We set $\mu_\alpha = 1$, $\mu_\gamma = 0.4$, and use two different initial conditions for $\mathbf{x}(t = 0)$: a low initial population (i.e., the elements of $\mathbf{x}$ are randomly drawn from a uniform distribution between 0 and 0.1) and a high initial population (i.e., the elements of $\mathbf{x}$ are randomly drawn from a uniform between 0.9 and 1).

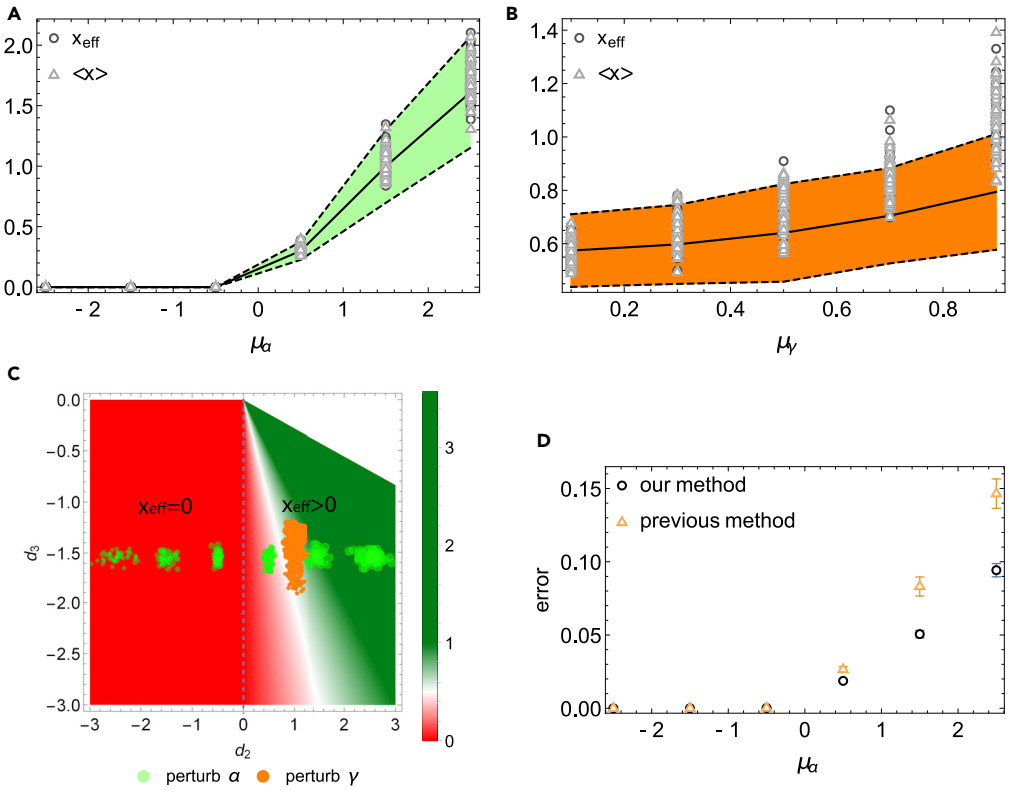

Figure 2. Results obtained from numerical simulation and theoretical predication as a function of changes on generalized Lotka-Volterra dynamics

The average population in the networked ecologic dynamics as a function of changes in (A) the mean μ_{α} of vector $\boldsymbol{\alpha}$ drawn from a normal distribution (and with fixed network A).

(B) The mean μ_{γ} of matrix γ_{ij} (and vector $\boldsymbol{\alpha}$ drawn from a normal distribution with mean μ_{α} and standard deviation $\sigma_{\alpha} = |\mu_{\alpha}/3|$ where $\mu_{\alpha} = 1$). In each panel, the solid black line represents the average of the analytical prediction $< x^{*}_{eff}(d_2, d_3) >$ over 50 realizations of the matrix **A** and vector $\boldsymbol{\alpha}$ through $d_2(\alpha_{eff})$ and $d_3(A_{eff})$.The dashed line represents the confidence level of three standard deviations.

(C) The density plot is given by the analytical form of x_{eff} as a function of d_2,d_3, whereas colored points shown on the varied perturbations collapse onto the manifold. For each perturbation type, the larger the points, the larger the perturbation.

(D) Error comparison between our method and the previous method by Gao et al. (Gao et al., 2016) as a function of the mean of vector $\boldsymbol{\alpha}$, whose elements are drawn from normal distribution.

We then perform numerical simulations to investigate how changes in the parameters of Equation (5) affect species abundances $\{x_1, x_2, \ldots, x_N\}$. The panels A and B of Figure 2 show the numerical simulation of the full N-dimensional GLV dynamics (where $<x> = \sum_{i=1}^{N} x_i/N$) when (1) decreasing the growth rate of species (for example, because of lack of resources or more unsuitable environmental conditions) and (2) decreasing the strength of mutualistic interactions, mimicking the possible effect of climate change (Saavedra et al., 2013; Morone et al., 2019). We find that the results from the numerical simulations collapse onto the manifold $x^{*}_{eff}(d_2, d_3)$ (Figure 2C) with relatively small error. To highlight the approximation errors, in Figures 2A and 2B we also show the analytical solution $x^{*}_{eff}(d_2, d_3)$. We note again that $d_2(\alpha_{eff})$ and $d_3(A_{eff})$ depend on the specific realization (of matrix A and vector $\boldsymbol{\alpha}$) and thus the black continuous lines represent the average $<x^{*}_{eff}(d_2, d_3)>$ (with colored area representing the three standard deviations) over the different realizations. In panel C of Figure 2 the predictions based on our framework are presented in terms of the effective state x_{eff}. Numerical simulations of both the complete dynamics and the macroscopic equation show that the system has only one stable state. In particular, we find that $\alpha_{eff} = 0$ is the critical value for such a transition. On the other hand, a decrease in μ_{γ} leads to a decrease in A_{eff}, which is associated with the extinction of some of the species and a slow decrease of both $<x>$ and x_{eff}. Therefore, an increase in both intrinsic growth rates (μ_{α}) and mutualistic strengths (μ_{γ}) is beneficial for species coexistence

(consistent with the collapse in mutualistic communities using critical slowing down methods (Dakos and Bascompte, 2014)).

Finally, we also compare the errors obtained between our method and the one of Gao et al. (Gao et al., 2016) as a function of μ_α. We find that the former performs similarly to the latter for $\mu_\alpha<0$, whereas for positive average growth rates $\mu_\alpha>0$ our approach outperforms the previous approach (Figure 2D). This result confirms (Tu et al., 2017) that the multi-dimensional reduction may also work for an interaction matrix with a mixture of positive and negative signs, thereby extending the scope of the previously proposed methods (Gao et al., 2016; Laurence et al., 2019).

Sustainability and effect of globalization on the food trade dynamics

In all the previous cases, we have considered complex dynamics, but with only one stable state for each set of parameters. We here apply our framework to a recently proposed case of bistable complex dynamics aimed at studying the effect of globalization on the sustainability of the global food system (Tu et al., 2019; Barthel and Isendahl, 2013; Suweis et al., 2015a). The proposed dynamics consider both local and imported resources and account for the interconnectedness existing in the global coupled food trade-production-consumption system, i.e.,

$$\frac{dx_i}{dt} = -\alpha_i c_i x_i + \left(\frac{\alpha_i c_i}{K_i^R} + \alpha_i\right) x_i^2 - \frac{\alpha_i}{K_i^R} x_i^3 - \delta\left(s_A^{out}\right)_i x_i + \delta \sum_j A_{ij} x_j \qquad \text{(Equation 6)}$$

where x_i is the resource volume of node i, and α_i, K_i^R, c_i are intrinsic growth parameter, carrying capacity and Allee parameter of the generalized logistic growth function describing the net dynamics of local food production and consumption; the matrix $\mathbf{A}$ is defined as $A_{i,j} = C_{i,j} K_i^L$, where K_i^L is the demand of country i; $C_{j,i}$ is a zero-diagonal adjacency matrix with size N, with non-null coefficients representing the existence and magnitude of a flux from node i to node j, and $(s_A^{out})_i$ is the out-degrees of node i of matrix $\mathbf{A}$(Tu et al., 2019).

The study estimated that the impact of globalization on the sustainable use of food resource depends on the structure of the food trade interaction network. In particular, Tu et al.(Tu et al., 2019) showed that if the network has an inverse relationship between in- and out-degrees of all nodes, then the globalization has a detrimental effect on sustainability. Here, we extend the previous work and analyze the sustainability accounting also for the node-specific dynamics (instead of using constant averaged parameters (Tu et al., 2019)). The effective equation of the model of resource dynamics is $\frac{dx_{eff}}{dt} = d_2 x_{eff} + d_3 x_{eff}^2 + d_4 x_{eff}^3$ where there are three effective parameters $d_2 = -\alpha_{eff} c_{eff} - \delta\eta_{eff} < 0$, $d_3 = \frac{\alpha_{eff} c_{eff}}{K_{eff}^R} + \alpha_{eff} > 0$, and $d_4 = -\frac{\alpha_{eff}}{K_{eff}^R} < 0$ and where $x_{eff} = \mathcal{L}(\mathbf{x})\alpha_{eff} = \mathcal{L}(\boldsymbol{\alpha})$, $c_{eff} = \mathcal{L}(\mathbf{c})$, $K_{eff}^R = \mathcal{L}(\mathbf{K_R})$, and $\eta_{eff} = \gamma_{eff} - \beta_{eff}$, with $\beta_{eff} = \mathcal{L}(\mathbf{s}^{in})$ and $\gamma_{eff} = \mathcal{L}(\mathbf{s}^{out})$ representing the effective import and export, respectively. We use the carrying capacities, food consumption, and production rates and the food trade network of the year 2013 (Tu et al., 2019). In this case, therefore, all the parameters of the model are node specific and fitted from the empirical data.

The effective equation predicts the existence of a bistable solution, one with $x_{eff} = 0$ and one with $x_{eff} > 0$. We now want to investigate the effect on globalization on the sustainability of the system ($x_{eff} > 0$). To do that, we investigate the effect of changes in food trade by increasing or decreasing the weight of the edges of the food trade network. In particular, to model the changes in globalization patterns we randomly multiply each weight by a factor r_{ij}, resulting in $A_{ij} \rightarrow r_{ij} A_{ij}$. The random variable r_{ij} is sampled from a uniform distribution with mean f_w. The result is that all weights are randomly modified, multiplied on average by a fraction f_w of their original value. To test the existence of bistable state, we use two different initial conditions $\mathbf{x}(t = 0) = \mathbf{z} * \mathbf{K}^R$: low initial condition, where $\mathbf{z}$ is vector randomly drawn from a uniform distribution between 0 and 0.1, and high initial condition, where $\mathbf{z}$ is a vector randomly drawn from a uniform distribution between 0.9 and 1.

Because α_{eff}, K_{eff}^R, c_{eff} do not vary with $f_w = 0.1, 0.4, 0.7, 1, 5, 10$ (see Figure S14A), while η_{eff} is quite sensitive to f_w (see Figure S14B), we focus on how the order parameter d_2 changes with the changes in the magnitude of trade, while keeping d_3, d_4 fixed. Solid lines in Figure 3 show the bifurcation diagram obtained from the effective equation described by Equation (3), whereas the points represent the x_{eff} calculated simulating the full dynamics given by Equation (6) and varying the intensity of trade by changing edge weights by a fraction equal to 0.1, 0.4, 0.7, 1, 5, and 10, respectively. We note that in this case the initial conditions do play a role, confirming the bistability predicted by our framework. When perturbation intensity is small

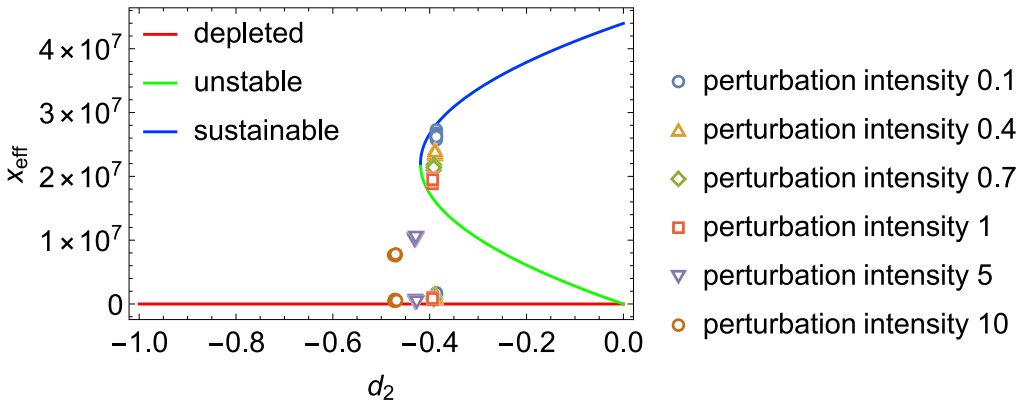

Figure 3. Results obtained from numerical simulation and theoretical predication as a function of changes on food trade dynamics

Dimensionality reduction of the food-trade model given by Equation (6). To model the changes in globalization patterns we randomly multiply each weight by a perturbation intensity factor r_{ij}, resulting in $A_{ij} \rightarrow r_{ij}A_{ij}$. The bifurcation diagram of the equilibrium states of x_{eff} as a function of effective parameter d_2, calculated with fixed d_3, d_4 that are fit from empirical data. The presented results are obtained from 50 realizations of the perturbation event.

so that its d_2 is smaller than critical value $d_2^{crt} = -\frac{\alpha_{eff}(c_{eff}+K_{eff}^R)}{4K_{eff}^R} = -0.4188$, bistability appears. On the other hand, we confirm the results of Tu et al.(Tu et al., 2019). In fact, we can see that by setting $\delta = 1*10^{-19}$ so that the present situation is at the edge of criticality between the sustainable and the unsustainable state, reducing the effect of globalization decreases the risk of the system collapse.

Effect of gene knockout and transcription inhibition to gene regulatory dynamics

We finally consider a biological example associated with gene expression. To model regulatory interactions between genes (Harush and Barzel, 2017; Hens et al., 2019), we consider the case where most of the genes are regulated by Michaelis-Menten (MM) type of interactions, whereas the remaining genes are involved in chemical binding (CB) interactions (or in both MM and CB couplings). The first subset of genes (for simplicity we consider the nodes from 1 to $\tilde{N}$) thus follows the celebrated Michaelis-Menten dynamics (Alon, 2006; Karlebach and Shamir, 2008) $\frac{dx_i}{dt} = -e_i x_i + \sum_j^N A_{ij}\frac{x_j}{x_j+1}$, where x_i represents the expression of gene i, whereas the first term on the right-hand side captures the degradation process and the second term accounts for genetic activation according to the Hill function (Karlebach and Shamir, 2008). The second subset of genes ($\tilde{N}+1 \le i \le N$) interacts through CB with coupling function $G_i(x_i, x_j) = -x_i * x_j$. Therefore, the corresponding high-dimensional equations for the gene expression with non-homogeneous dynamics mechanisms are

$$\begin{cases} \frac{dx_i}{dt} = -e_i x_i + \sum_j^N A_{ij}\frac{x_j}{1+x_j}, 0 \le i \le \tilde{N} \\ \frac{dx_i}{dt} = -e_i x_i + \sum_j^N A_{ij}(-x_i * x_j), \tilde{N}+1 \le i \le N \end{cases} \quad \text{(Equation 7)}$$

We then apply our dimensionality reduction to Equation (7). Because the coupling-dynamics $G_i(x_i, x_j) = \frac{x_j}{x_j+1}$ are not a polynomial, we use the MATLAB toolbox Chebfun (Trefethen, 2013; Driscoll et al., 2014) to calculate the Chebyshev coefficients and then rescale it to the desired interval (depending on the desired accuracy, see Transparent methods, sections Chebyshev approximation theory and Validation of the Chebyshev approximation). Thus, we obtain the Chebyshev's polynomial approximation, $c_{i,1} + c_{i,2}x_j + c_{i,3}x_j^2 + c_{i,4}x_j^3 + c_{i,5}x_j^4$, where the Chebyshev coefficients are $c_{i,1} = 0$, $c_{i,2} = 0.597$, $c_{i,3} = -0.154$, $c_{i,4} = 0.0167$, $c_{i,5} = -0.000645$ when $0 \le i \le \tilde{N}$ (see Figure S3 A). The low-dimensional effective equation is $\frac{dx_{eff}}{dt} = d_1 x_{eff}^0 + d_2 x_{eff}^1 + d_3 x_{eff}^2 + d_4 x_{eff}^3 + d_5 x_{eff}^4$ where $d_1 = A_{eff}C_{eff}^1$, $d_2 = -e_{eff} + A_{eff}C_{eff}^2$, $d_3 = A_{eff}C_{eff}^3$, $d_4 = A_{eff}C_{eff}^4$, and $d_5 = A_{eff}C_{eff}^5$ where $C_{eff}^1 = \mathcal{L}([0,0,\ldots]) = 0$, $C_{eff}^2 = \mathcal{L}([0.597,\ldots,0.597,0,\ldots,0])$, $C_{eff}^3 = \mathcal{L}([-0.154,\ldots,-0.154,-1,\ldots,-1])$, $C_{eff}^4 = \mathcal{L}([0.0167,\ldots,0.0167,0,\ldots,0])$, and $C_{eff}^5 = \mathcal{L}([-0.000645,\ldots,-0.000645,0,\ldots,0])$.

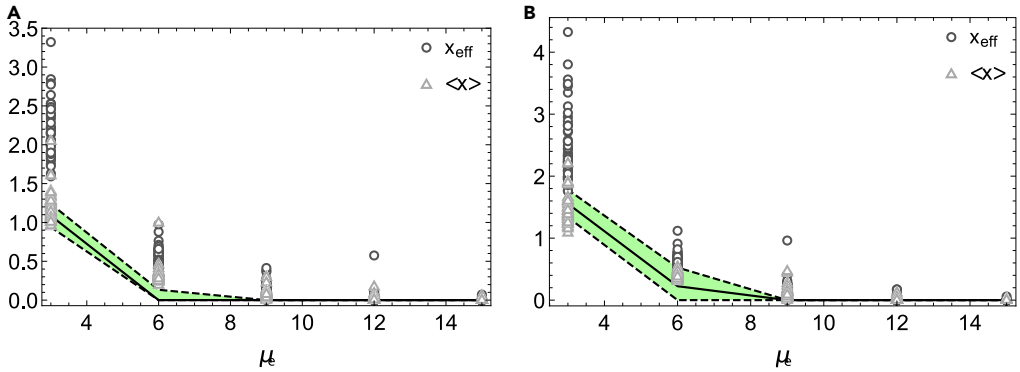

Figure 4. Results obtained from numerical simulation and theoretical predication as a function of changes on gene regulatory dynamics

Dimensionality reduction for non-homogeneous dynamics mechanisms of gene regulations given by (A) Equation (7) and (B) Equation (8). Black and gray markers represent the numerical weighted average x_{eff} and average <x> obtained from the simulation of the full N-dimensional coupled dynamics, as a function of changes in the mean μ_e of the vector **e** drawn from a uniform distribution. The black lines indicate the analytical solution given by $<x^*_{eff}(e_{eff},A_{eff})>$. We highlight that e_{eff} and A_{eff} depend on the specific realization (of matrix A and vector **e**) and thus we compute the average $< x^*_{eff}(e_{eff},A_{eff})>$ (with colored green area representing the three standard deviations) over 50 different realizations.

We also explore the case where both linear regulation through promoter genes and chemical binding interactions present in a small subgroup of nodes ($\tilde{N}+1\leq i\leq N$). In this case, the coupling-dynamics reads as, i.e., $G_i(x_i,x_j) = (1-x_i)*x_j$, while the corresponding full high-dimensional equation becomes

$$\begin{cases} \dfrac{dx_i}{dt} = -e_i x_i + \sum_j^N A_{ij}\dfrac{x_j}{1+x_j}, 0\leq i\leq \tilde{N} \\ \dfrac{dx_i}{dt} = -e_i x_i + \sum_j^N A_{ij}(1-x_i)x_j, \tilde{N}+1\leq i\leq N \end{cases} \quad \text{(Equation 8)}$$

The low-dimensional effective equation is $\frac{dx_{eff}}{dt} = d_1 x^0_{eff} + d_2 x^1_{eff} + d_3 x^2_{eff} + d_4 x^3_{eff} + d_5 x^4_{eff}$ where $d_1 = A_{eff}C^1_{eff}$, $d_2 = -e_{eff} + A_{eff}C^2_{eff}$, $d_3 = A_{eff}C^3_{eff}$, $d_4 = A_{eff}C^4_{eff}$, and $d_5 = A_{eff}C^5_{eff}$ where $C^1_{eff} = \mathcal{L}([0,0,\ldots]) = 0$, $C^2_{eff} = \mathcal{L}([0.597,\ldots,0.597,1,\ldots,1])$, $C^3_{eff} = \mathcal{L}([-0.154,\ldots,-0.154,-1,\ldots,-1])$, $C^4_{eff} = \mathcal{L}([0.0167,\ldots,0.0167,0,\ldots,0])$, and $C^5_{eff} = \mathcal{L}([-0.000645,\ldots,-0.000645,0,\ldots,0])$.

For the regulatory model, we generate a constant scale-free network with scale parameter 3 and size $N = 100$ and assume that $\tilde{N} = 80$ in Equation (7) or (8). We set $\mathbf{e} = (e_1,\ldots,e_N)^T$ as a vector whose elements are drawn from a uniform distribution between 0 and $2\mu_e$, i.e., μ_e is the average degradation rate. We set $\mu_e = 3$ and use two different initial conditions for $\mathbf{x}(t=0)$: a low initial gene expression value drawn from a uniform distribution between 0 and 0.1, and a high initial gene expression drawn from a uniform distribution between 0.9 and 1.

Although there are five parameters d_1,d_2,d_3,d_4,d_5, there are only two effective parameters e_{eff},A_{eff}. Therefore, for visualization, we consider the three-dimensional space composed of e_{eff},A_{eff},x_{eff}. Figure 4 shows the results when we vary the average degradation rate μ_e of the full N-dimensional mixed equation. We find that our method can be applied to non-homogeneous dynamics mechanisms where different nodes are driven by different self and coupling-dynamics (see also Transparent methods, section Non-homogeneous dynamics mechanisms).

DISCUSSION

The dynamics of complex networked systems are often difficult to investigate in their complete parameter space. The seminal work by Gao et al.(Gao et al., 2016) and successive ones (Laurence et al., 2019) provided a mean-field representation of such dynamics that served as a one-dimensional manifold for the high-dimensional networked dynamics. Such a framework, however, hinged on the assumption that all nodes in the network are similar (low heterogeneity of the model parameters) and have the same self-dynamics

and coupling-dynamics, which limited the applicability of this framework. Our extension of their framework lends itself to the study of the collapse or functioning of any networked systems, accounting also for the full heterogeneity in node-specific self- and coupling-dynamics. In fact, under our assumptions, we can map the high-dimensional equation onto a low-dimensional dynamic in only one (effective) state variable and S effective parameters, and it works well in different theoretical models and heterogeneous networks (see Transparent methods, section Extended validation, Non-homogeneous dynamics mechanisms and Effect of heterogeneity). We can then use these manifold dynamics to investigate the system's response to changes in the parameters and determine the steady states of the system and the possible existence of transitions between functioning or sustainable stables, including possible critical transitions in the case of bifurcating bistable dynamics. Our framework can address not only non-homogeneous dynamic parameters where all nodes interact through the same mechanisms (i.e., expressed by the same functional form, though with different parameters) but also the case of non-homogeneous dynamics whereby the functional form of self-dynamics $F(x)$ and coupling-dynamics $G(x, y)$ differ across the nodes. The numerical simulation of real-world examples presented in the Results section demonstrates that our framework works well both in the case of homogeneous and heterogeneous dynamics (see Transparent methods, section Heterogeneous networks).

In many cases, the analytical expressions of the self-dynamics $F_i(x_i)$ and coupling-dynamics $G_i(x_i, x_j)$ of the systems may be unknown. However, we note that our framework also works if these functions can be calculated from the empirical data, i.e., $\{x_m, F_i(x_m)\}$ and $\{x_m, y_m, G_i(x_m, y_m)\}$, where $m \in \{1, \ldots, n\}$ and n is the sample number. In fact, in this case we can still construct interpolating polynomials, $\sum_{k=1}^{n} b_k x^{(k-1)}$ and $\sum_{p,q=1}^{n/2} d_{p,q} x^{(p-1)} y^{(q-1)}$, and use them as the self-dynamics and coupling-dynamics of node i. In fact, in many real-world complex cases, we have times series of the empirical data for each of the system's variables (e.g. species abundances), but we typically do not know the functional form of the self-dynamics and coupling-dynamics that can simulate the underlying processes. In this case we may directly perform a polynomial fitting on the data, thus constructing $F_i(x_i)$ and $G_i(x_i, x_j)$; then we can apply our framework to predict the system's behavior, a function of polynomial coefficients. Moreover, in high-dimensional systems, the critical slowing down method is difficult to apply because it would require a large number of numerical simulations to investigate how the equilibria of the system change by varying one parameter at time while keeping the others fixed, making such an analysis is often a computationally prohibitive task, especially for large networks and in the presence of nonlinear self-dynamics and coupling-dynamics (Sornette, 2006; Scheffer et al., 2009, 2012). In contrast, our framework provides an analytical method that is computationally feasible, thus further facilitating the study, design, or manage networked systems and the identification of criteria to optimize their resilience under a given set of constraints.

All in all, our methodology provides (approximated) results for dimensionality reduction that are applicable to a broader set of systems and dynamics and exploited in different contexts ranging from ecology to epidemiology and the study of critical transitions.

Limitations of the study

Our method also presents some limitations that need to be carefully considered and tested. First of all, the proposed framework is based on the mean-field approximation of Gao et al.(Gao et al., 2016) and thus works well when the network connecting the system components has negligible degree correlation and its weights are not too heterogeneous (Tu et al., 2017). Moreover, in the use of the Hadamard product approximation, the parameters of the self- and couple dynamics should not be "too" heterogeneous; otherwise, the approximation will fail (see Transparent methods, section Validation of the Hadamard product). In other terms, the effective value of the Hadamard product of two vectors $\mathcal{L}(\mathbf{x}\circ\mathbf{y})$ should be close enough to the product of effective values of the two vectors $\mathcal{L}(\mathbf{x})\mathcal{L}(\mathbf{y})$, and this condition holds if $\mathbf{x}$ and $\mathbf{y}$ both have a small coefficient of variation. Then, the order of the Chebyshev polynomial should be sufficiently high to capture the complex behaviors of the dynamics (see Transparent methods, section Validation of the Chebyshev approximation). However, there are no *a-priori* criteria that can be used to determine a suitable order of this polynomial expansion. In addition, our method is not applicable if the coupling-dynamics are $G_{ij}(x_i, x_j)$ instead of $G_i(x_i, x_j)$. In fact, in the case of a networked system $\frac{dx_i}{dt} = F_i(x_i) + \sum_j^N A_{ij} G_{ij}(x_i, x_j)$, if the degree correlations of the network $\mathbf{A}$ are weak, then we make the approximation $\sum_j^N A_{i,j} G_{ij}(x_i, x_j) \approx s_i^{in} \mathcal{L}(G_{ij}(x_i, \mathbf{x}))$ and because $\mathcal{L}(G_{ij}(x_i, \mathbf{x})) \neq G_{ij}(x_i, \mathcal{L}(\mathbf{x}))$, further application of our framework would not be possible. Moreover, the fact that the low-dimensional effective system is stable does not guarantee that

the high-dimensional networked system is also stable. If in the high-dimensional networked system an equilibrium point is stable, the corresponding equilibrium will be stable also in the low-dimensional effective system, whereas the other way around is not necessarily true. For this reason, when we apply our framework in the case of non-homogenous dynamics mechanisms in *N*-dimensional complex systems we need to be very careful. In fact, in the latter case, it may be very difficult to find a configuration of the initial model parameters in which the *N*-dimensional system is stable. However, applying the dimensionality reduction when the *N*-dimensional system is unstable gives confounding results, as the effective dynamics may be stable.

Resource availability

Lead contact

Chengyi Tu (chengyitu@berkeley.edu).

Materials availability

This study did not generate new unique reagents.

Data and code availability

The datasets and ready-to-use notebook codes to reproduce the results presented in the current study are available in Mendeley with the access code nnxxxmhzgw (https://data.mendeley.com/datasets/nnxxxmhzgw).

METHODS

All methods can be found in the accompanying Transparent methods supplemental file.

SUPPLEMENTAL INFORMATION

Supplemental Information can be found online at https://doi.org/10.1016/j.isci.2020.101912.

ACKNOWLEDGMENTS

C.T. acknowledges Microsoft AI for Earth and Yunnan University project C176210103. S.S. acknowledges the University of Padova for International Cooperation Grant 2019–2020.

AUTHOR CONTRIBUTIONS

C.T. and S.S. designed the research, the analysis and the manuscript with critical input from P.D. C.T. implemented the model and performed the analysis. S.S. and P.D. contributed to the development and generalization of the framework. All authors wrote the manuscript.

DECLARATION OF INTERESTS

The authors declare no competing interests.

Received: July 29, 2020
Revised: November 6, 2020
Accepted: December 3, 2020
Published: January 22, 2021

REFERENCES

Allesina, S., and Tang, S. (2012). Stability criteria for complex ecosystems. Nature *483*, 205–208.

Alon, U. (2006). An Introduction to Systems Biology: Design Principles of Biological Circuits (CRC press).

Arnoldi, J.-F., Loreau, M., and Haegeman, B. (2016). Resilience, reactivity and variability: a mathematical comparison of ecological stability measures. J. Theor. Biol. *389*, 47–59.

Barlow, J., Lennox, G.D., Ferreira, J., Berenguer, E., Lees, A.C., Nally, R.M., Thomson, J.R., Ferraz, S.F.D.B., Louzada, J., Oliveira, V.H.F., et al. (2016). Anthropogenic disturbance in tropical forests can double biodiversity loss from deforestation. Nature *535*, 144–147.

Barthel, S., and Isendahl, C. (2013). Urban gardens, agriculture, and water management: Sources of resilience for long-term food security in cities. Ecol. Econ. *86*, 224–234.

Boguna, M., Castellano, C., and Pastorsatorras, R. (2013). Nature of the epidemic threshold for the susceptible-infected-susceptible dynamics in networks. Phys. Rev. Lett. *111*, 068701.

Boyd, J.P. (2001). Chebyshev and Fourier Spectral Methods (Courier Corporation).

Ceballos, G., Ehrlich, P.R., Barnosky, A.D., García, A., Pringle, R.M., and Palmer, T.M. (2015). Accelerated modern human–induced species

losses: entering the sixth mass extinction. Sci. Adv. *1*, e1400253.

Cenci, S., Song, C., and Saavedra, S. (2017). Rethinking the Importance of Ecological Networks through the Glass of Environmental Variations. bioRxiv, 219691.

Dakos, V., and Bascompte, J. (2014). Critical slowing down as early warning for the onset of collapse in mutualistic communities. PNAS *111*, 17546–17551.

Drever, C.R., Peterson, G., Messier, C., Bergeron, Y., and Flannigan, M. (2006). Can forest management based on natural disturbances maintain ecological resilience. Can. J. For. Res. *36*, 2285–2299.

Driscoll, T.A., Hale, N., and Trefethen, L.N. (2014). Chebfun Guide (Pafnuty Publications).

Gao, J., Barzel, B., and Barabási, A.-L. (2016). Universal resilience patterns in complex networks. Nature *530*, 307.

Gauthier, S., Bernier, P., Kuuluvainen, T., Shvidenko, A.Z., and Schepaschenko, D.G. (2015). Boreal forest health and global change. Science *349*, 819–822.

Grilli, J., Adorisio, M., Suweis, S., Barabás, G., Banavar, J.R., Allesina, S., and Maritan, A. (2017). Feasibility and coexistence of large ecological communities. Nat. Commun. *8*, 14389.

Harush, U., and Barzel, B. (2017). Dynamic patterns of information flow in complex networks. Nat. Commun. *8*, 1–11.

Hens, C., Harush, U., Haber, S., Cohen, R., and Barzel, B. (2019). Spatiotemporal signal propagation in complex networks. Nat. Phys. *15*, 403–412.

Holling, C.S. (1973). Resilience and stability of ecological systems. Annu. Rev. Ecol. Evol. Syst. *4*, 1–23.

Huang, S., Eichler, G., Bar-Yam, Y., and Ingber, D.E. (2005). Cell fates as high-dimensional attractor states of a complex gene regulatory network. Phys. Rev. Lett. *94*, 128701–129600.

Hughes, T.P., Kerry, J.T., Baird, A.H., Connolly, S.R., Dietzel, A., Eakin, C.M., Heron, S.F., Hoey, A.S., Hoogenboom, M.O., and Liu, G. (2018). Global warming transforms coral reef assemblages. Nature *556*, 492–496.

Isella, L., Stehle, J., Barrat, A., Cattuto, C., Pinton, J., and Den Broeck, W.V. (2011). What's in a crowd? Analysis of face-to-face behavioral networks. J. Theor. Biol. *271*, 166–180.

Johnson, C.N., Balmford, A., Brook, B.W., Buettel, J.C., Galetti, M., Guangchun, L., and Wilmshurst, J.M. (2017). Biodiversity losses and conservation responses in the Anthropocene. Science *356*, 270–275.

Karlebach, G., and Shamir, R. (2008). Modelling and analysis of gene regulatory networks. Nat. Rev. Mol. Cell. Biol. *9*, 770–780.

Lara, C. (2006). Temporal dynamics of flower use by hummingbirds in a highland temperate forest in Mexico. Ecoscience *13*, 23–29.

Laurence, E., Doyon, N., Dubé, L.J., and Desrosiers, P. (2019). Spectral dimension reduction of complex dynamical networks. Phys. Rev. X *9*, 011042.

Lyapunov, A.M. (1992). The general problem of the stability of motion. Int. J. Control *55*, 531–534.

Mason, J.C., and Handscomb, D.C. (2002). Chebyshev Polynomials (Chapman And Hall/Crc).

Melbourne, B.A., and Hastings, A. (2008). Extinction risk depends strongly on factors contributing to stochasticity. Nature *454*, 100–103.

Morone, F., Del Ferraro, G., and Makse, H.A. (2019). The k-core as a predictor of structural collapse in mutualistic ecosystems. Nat. Phys. *15*, 95–102.

Oliver, T.H., Heard, M.S., Isaac, N.J.B., Roy, D.B., Procter, D., Eigenbrod, F., Freckleton, R., Hector, A., Orme, C.D.L., and Petchey, O.L. (2015). Biodiversity and resilience of ecosystem functions. Trends Ecol. Evol. *30*, 673–684.

Pan, L., Yang, D., Wang, W., Cai, S., Zhou, T., and Lai, Y.-C. (2020). Phase diagrams of interacting spreading dynamics in complex networks. Phys. Rev. Res. *2*, 023233.

Pastor-Satorras, R., Castellano, C., Van Mieghem, P., and Vespignani, A. (2015). Epidemic processes in complex networks. Rev. Mod. Phys. *87*, 925.

Rieger, C.G., Gertman, D.I., and Mcqueen, M.A. (2009). Resilient control systems: next generation design research. In 2nd Conference on Human System Interactions (IEEE), pp. 632–636.

Rossi, R.A., and Ahmed, N.K. (2015). The Network Data Repository with Interactive Graph Analytics and Visualization (AAAI).

Saavedra, S., Rohr, R.P., Dakos, V., and Bascompte, J. (2013). Estimating the tolerance of species to the effects of global environmental change. Nat. Commun. *4*, 2350.

Scheffer, M., Bascompte, J., Brock, W.A., Brovkin, V., Carpenter, S.R., Dakos, V., Held, H., Van Nes, E.H., Rietkerk, M., and Sugihara, G. (2009). Early-warning signals for critical transitions. Nature *461*, 53.

Scheffer, M., Carpenter, S.R., Lenton, T.M., Bascompte, J., Brock, W., Dakos, V., Van De Koppel, J., Van De Leemput, I.A., Levin, S.A., and Van Nes, E.H. (2012). Anticipating critical transitions. Science *338*, 344–348.

Serván, C.A., Capitán, J.A., Grilli, J., Morrison, K.E., and Allesina, S. (2018). Coexistence of many species in random ecosystems. Nat. Ecol. Evol. *2*, 1237–1242.

Sornette, D. (2006). Critical Phenomena in Natural Sciences: Chaos, Fractals, Selforganization and Disorder: Concepts and Tools (Springer Science & Business Media).

Suweis, S., Carr, J.A., Maritan, A., Rinaldo, A., and D'odorico, P. (2015a). Resilience and reactivity of global food security. Proc. Natl. Acad. Sci. U S A *112*, 6902–6907.

Suweis, S., and D'odorico, P. (2014). Early warning signs in social-ecological networks. PLoS One *9*, e101851.

Suweis, S., Grilli, J., Banavar, J.R., Allesina, S., and Maritan, A. (2015b). Effect of localization on the stability of mutualistic ecological networks. Nat. Commun. *6*, 10179.

Suweis, S., Simini, F., Banavar, J.R., and Maritan, A. (2013). Emergence of structural and dynamical properties of ecological mutualistic networks. Nature *500*, 449–452.

Thibeault, V., St-Onge, G., Dubé, L.J., and Desrosiers, P. (2020). Threefold Way to the Dimension Reduction of Dynamics on Networks: An Application to Synchronization. arXiv.

Trefethen, L.N. (2013). Approximation Theory and Approximation Practice (Siam).

Tu, C., Grilli, J., Schuessler, F., and Suweis, S. (2017). Collapse of resilience patterns in generalized Lotka-Volterra dynamics and beyond. Phys. Rev. E *95*, 062307.

Tu, C., Suweis, S., and D'odorico, P. (2019). Impact of globalization on the resilience and sustainability of natural resources. Nat. Sustain. *2*, 283–289.

Walker, B., Holling, C.S., Carpenter, S.R., and Kinzig, A.P. (2004). Resilience, adaptability and transformability in social–ecological systems. Ecol. Soc. *9*, 5.

Woods, D.D. (2006). Resilience Engineering: Concepts and Precepts (Ashgate Publishing, Ltd).

iScience, Volume *24*

Supplemental Information

Dimensionality reduction of complex dynamical systems

Chengyi Tu, Paolo D'Odorico, and Samir Suweis

Supplementary Figures

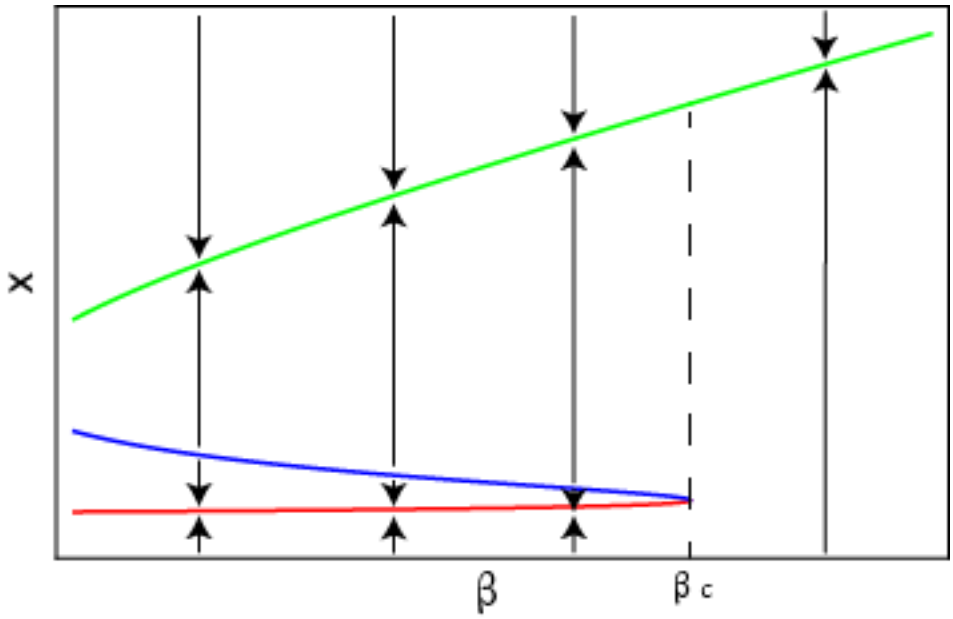

Figure S1. An example of resilience function for a one-dimensional equation displaying a bifurcation. Related to Fig. 1. *The green and red branches represent desired and undesired stable fixed points, respectively. The blue branch represents an unstable state. If $\beta > \beta_c$, there is only a single stable state (green curve); otherwise, there is a desired stable state (green curve) and another undesired state (red curve).*

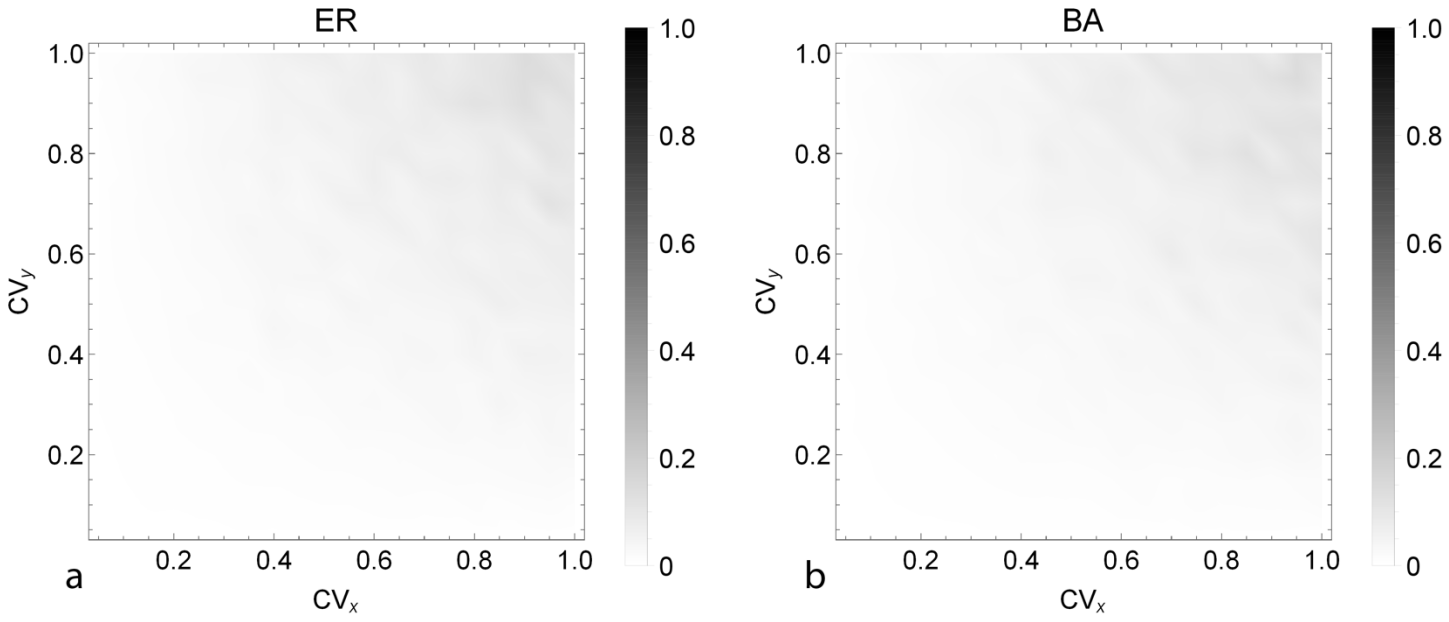

Figure S2. Testing the validation of the Hadamard product with different CVx (coefficient of variation of vector $\mathbf{x}$) and CVy (coefficient of variation of vector $\mathbf{y}$). Related to Fig. 1. *(a) ER network with size 50 and connectivity 0.2; (b) BA*

network with size 50 and parameter 10. The elements of vector $\mathbf{x}$ *are drawn from a normal distribution with mean 1 and standard deviation between 0 and 1, and the same is true of vector* $\mathbf{y}$ *.*

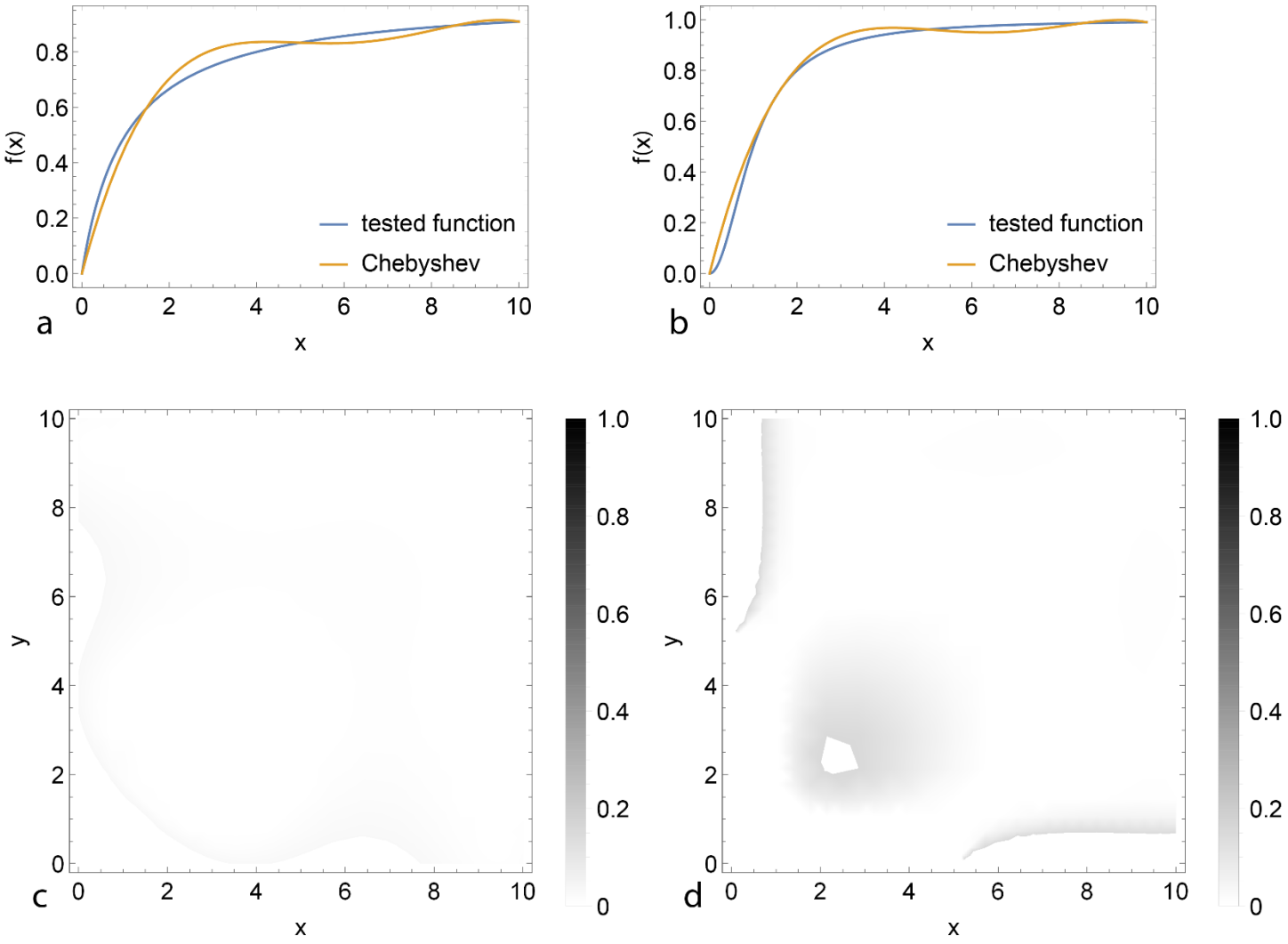

Figure S3. Testing the Chebyshev approximation with one-variable and two-variable Chebyshev polynomials. Related to Fig. 1. *(a) Comparison between the tested function* $\frac{x^1}{x^1+1}$ *and its Chebyshev approximation with degree 5; (b) comparison between the tested function* $\frac{x^2}{x^2+1}$ *and its Chebyshev approximation with degree 5; (c) relative error between the tested function* $\frac{x^1 y^1}{x^1+y^1+1}$ *and its Chebyshev approximation with degree 5; (d) relative error between the tested function* $\frac{x^2 y^2}{x^2+y^2+1}$ *and its Chebyshev approximation with degree 5.*

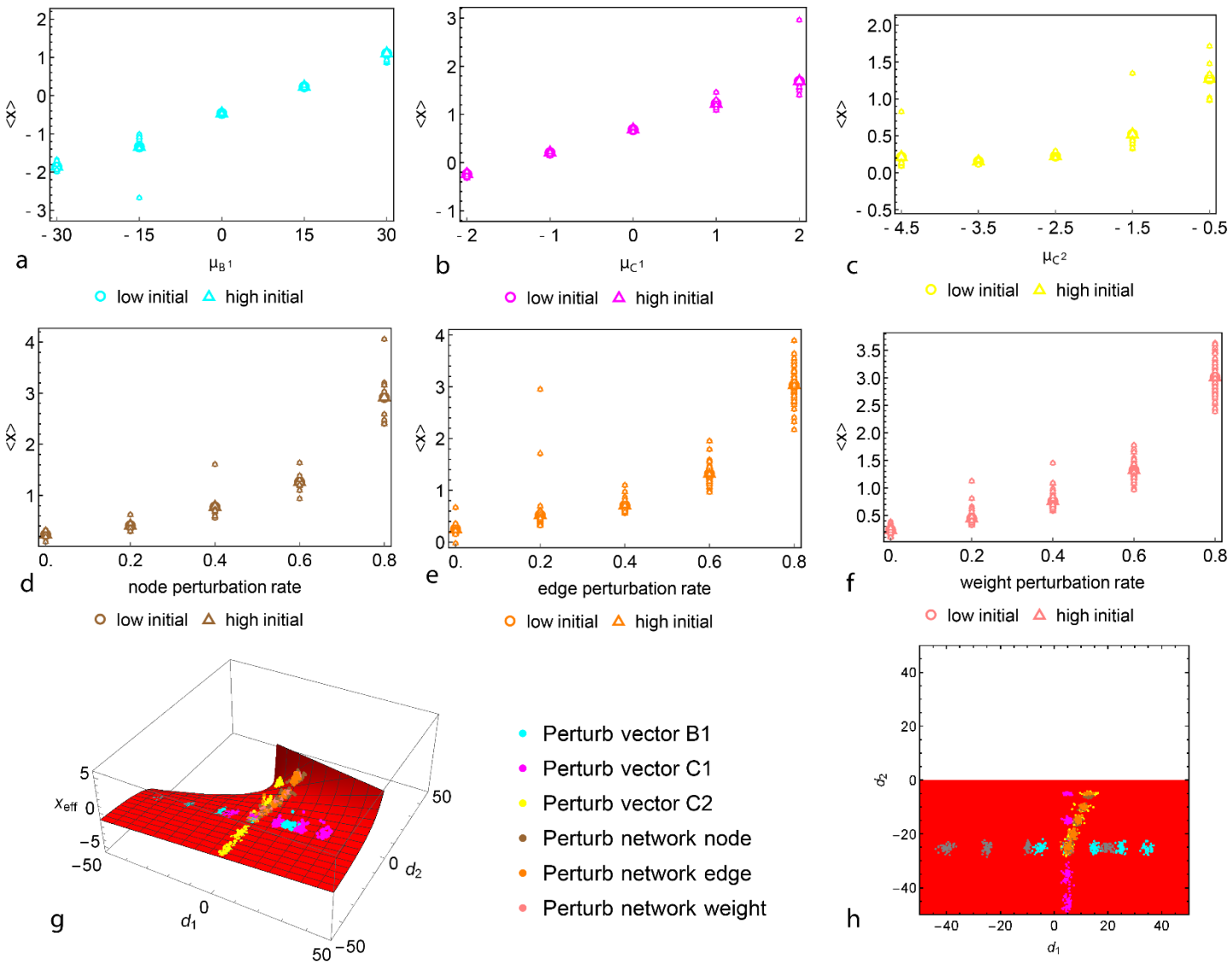

Figure S4. Results obtained from numerical simulation and theoretical predication as a function of changes on case d1, d2. Related to Fig. 1. *Average state of the system as a function of changes in (a) the mean* μ_{B^1} *of vector* B^1 *; (b) the mean* μ_{C^1} *of vector* C^1*; (c) the mean* μ_{C^2} *of vector* C^2*; (d) the rate of removal of network nodes; (e) the rate of removal of network edges; (f) the rate of reduction of network weights. For each case, we run 50 simulations, and the large marker represents their average. (g) Effective state of the system in three-dimensional space composed of the state variable* x_{eff} *and effective parameters* d_1, d_2*. Each colored surface represents one stable state in the manifold. The points representing the steady states in the complete multidimensional model as a function of changes in the parameters of the dynamics collapse onto the manifold. (h) The projection of (g) by eliminating the dimension* x_{eff}*.*

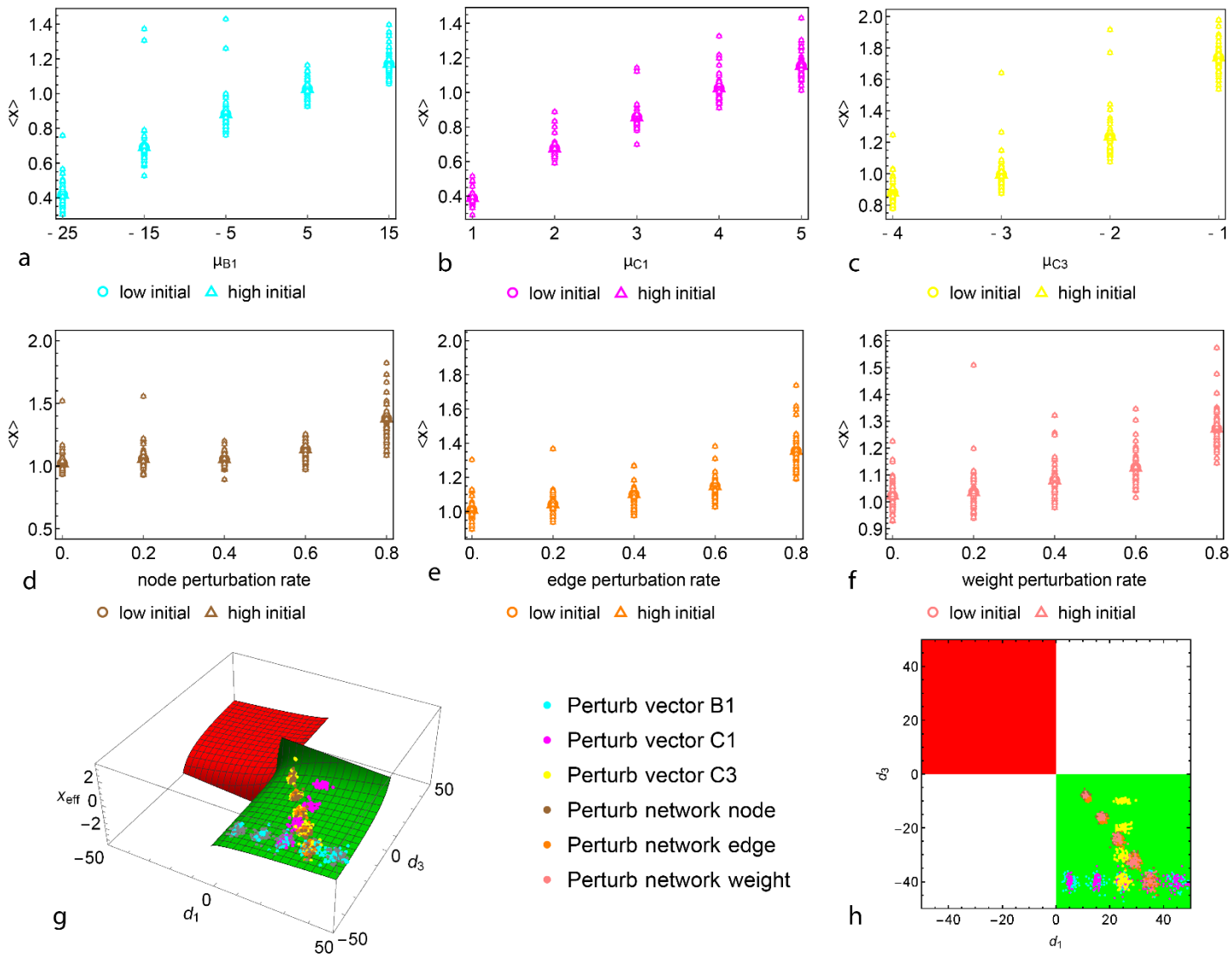

Figure S5. Results obtained from numerical simulation and theoretical predication as a function of changes on case d1, d3. Related to Fig. 1. *Average state of the system as a function of changes in (a) the mean* μ_{B^1} *of vector* B^1*; (b) the mean* μ_{C^1} *of vector* C^1*; (c) the mean* μ_{C^3} *of vector* C^3*; (d) the rate of removal of network nodes; (e) the rate of removal of network edges; (f) the rate of reduction of network weights. (g) Effective state of the system in three-dimensional space composed of the state variable* x_{eff} *and the effective parameters* d_1, d_3*. Each colored surface represents one stable state in the manifold. The points representing the steady states in the complete multidimensional model as a function of changes in the parameters of the dynamics collapse onto the manifold. (h) The projection of (g) by eliminating the dimension* x_{eff} *.*

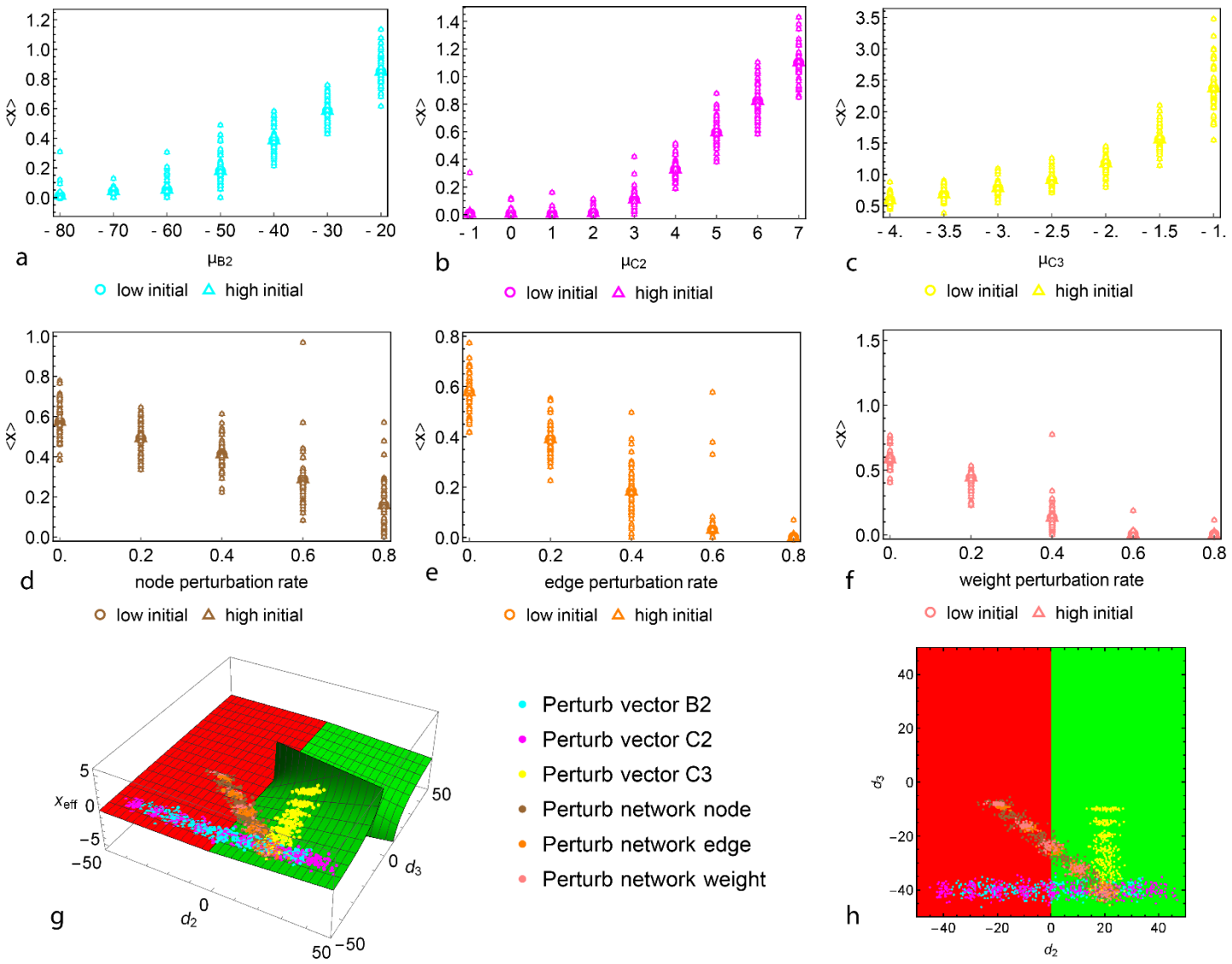

Figure S6. Results obtained from numerical simulation and theoretical predication as a function of changes on case d2, d3. Related to Fig. 1. *Average state of the system as a function of changes in (a) the mean* μ_{B^2} *of vector* B^2*; (b) the mean* μ_{C^2} *of vector* C^2*; (c) the mean* μ_{C^3} *of vector* C^3*; (d) the rate of removal of network nodes; (e) the rate of removal of network edges; (f) the rate of reduction of network weights. For each case, we run 50 simulations, and the large marker represents their average. (g) Effective state of the system in three-dimensional space composed of the state variable* x_{eff} *and the effective parameters* d_2, d_3*. Each colored surface represents one stable state in the manifold. The points representing the steady states in the complete multidimensional model as a function of changes in the parameters of the dynamics collapse onto the manifold. (h) The projection of (g) by eliminating the dimension* x_{eff}*.*

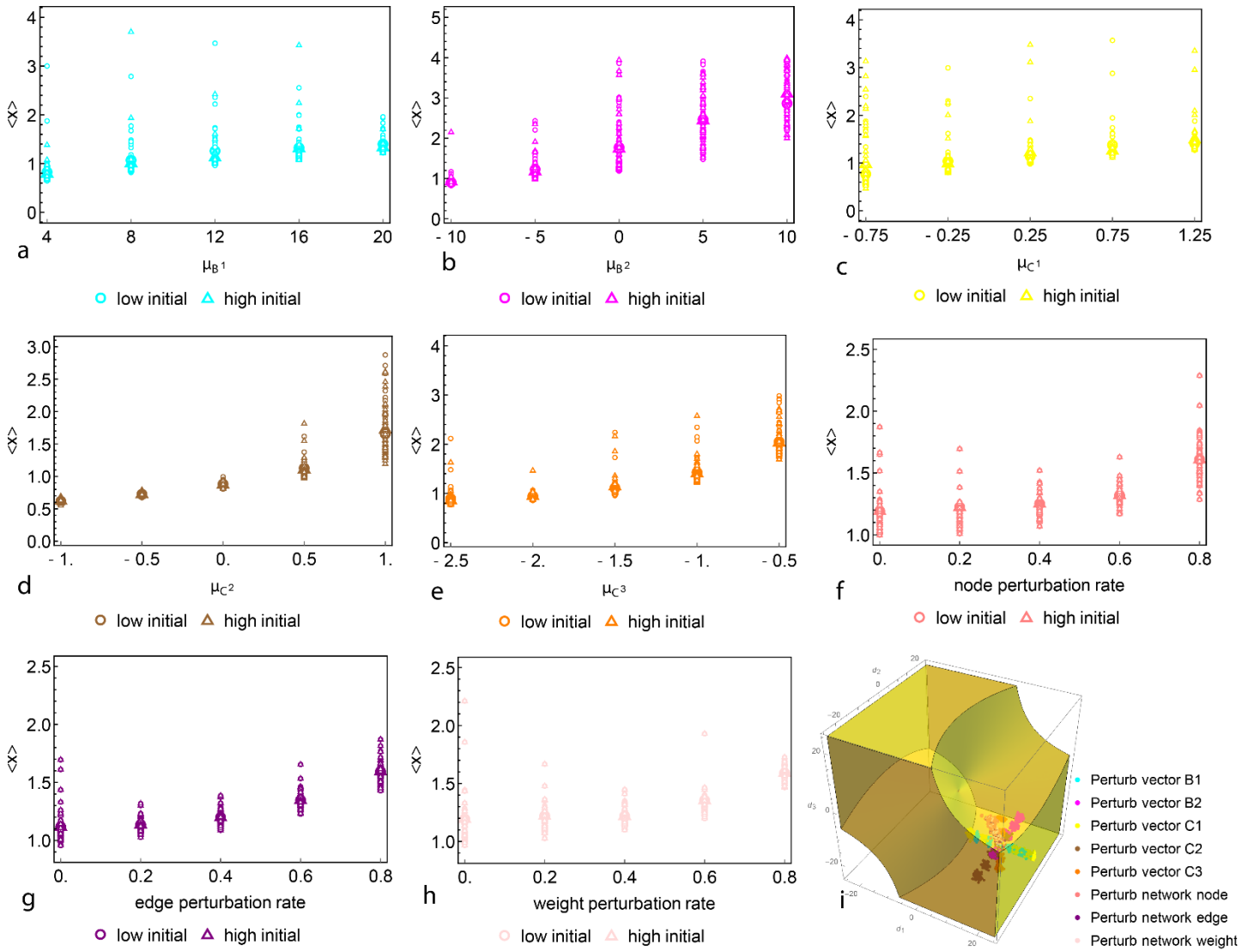

Figure S7. Results obtained from numerical simulation and theoretical predication as a function of changes on case d1, d2, d3. Related to Fig. 1. *Average state of the system as a function of changes in (a) the mean* μ_{B^1} *of vector* B^1*; (b) the mean* μ_{B^2} *of vector* B^2*; (c) the mean* μ_{C^1} *of vector* C^1*; (d) the mean* μ_{C^2} *of vector* C^2*; (e) the mean* μ_{C^3} *of vector* C^3*; (f) the rate of removal of network nodes; (g) the rate of removal of network edges; (h) the rate of reduction of network weights. For each case, we run 50 simulations, and the large marker represents their average. (i) Projection of the effective function by eliminating the dimension* x_{eff}*. The three dimensions are the effective parameters* d_1, d_2, d_3*.*

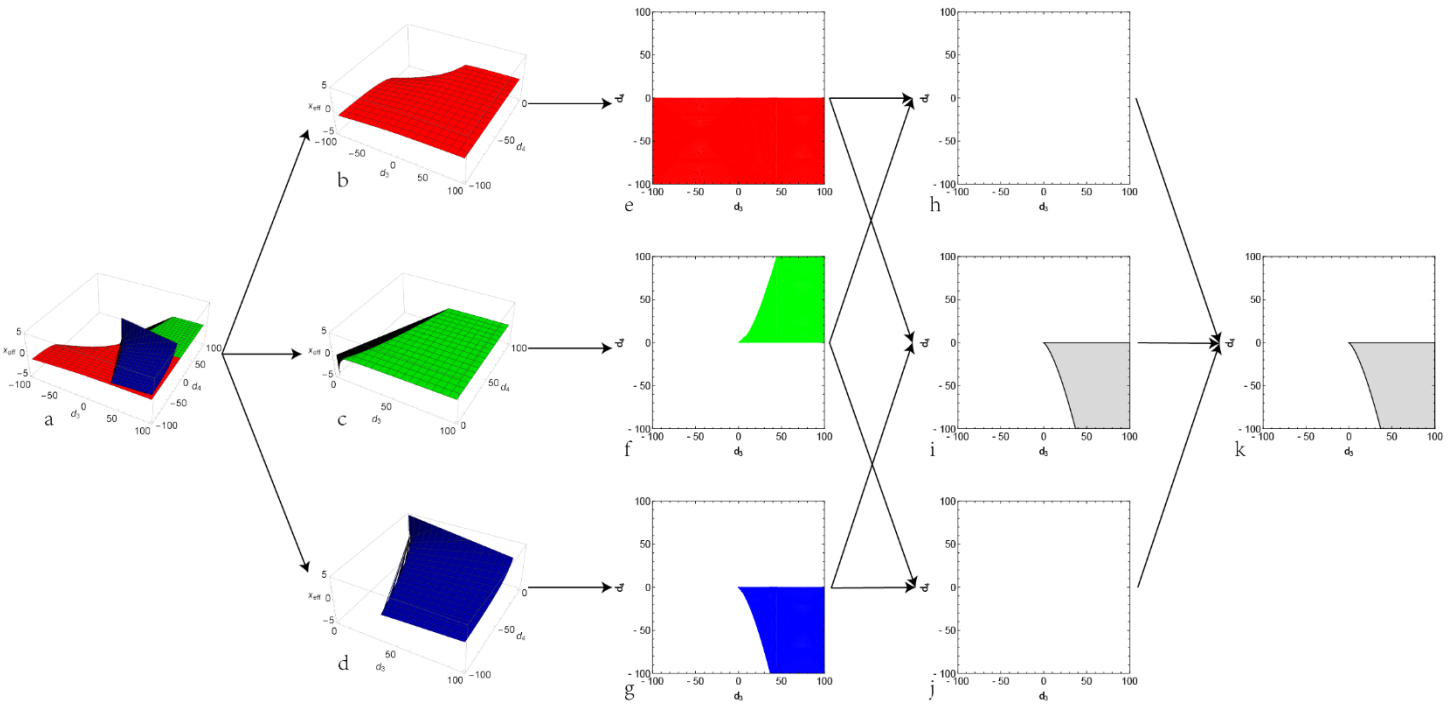

Figure S8. Illustration of the general resilience framework to identify the bi-stability region and critical boundary. Related to Fig. 1. *(a) Three-dimensional effective bifurcation diagram with state variable* x_{eff} *and effective parameters* d_3, d_4*. Each colored surface represents one region of the stable state. (b-d) Each colored surface is shown in a single three-dimensional space. (e-g) The projection of (b-d) by eliminating the dimension* x_{eff}*. (h) The intersection of the regions shown in (e) and (f). (i) The intersection of the regions shown in (e) and (g). (j) The intersection of the regions shown in (f) and (g). (k) The union of the regions shown in (h-j). Black represents the critical boundary, and gray represents the bi-stability region, which has more than one stable state.*

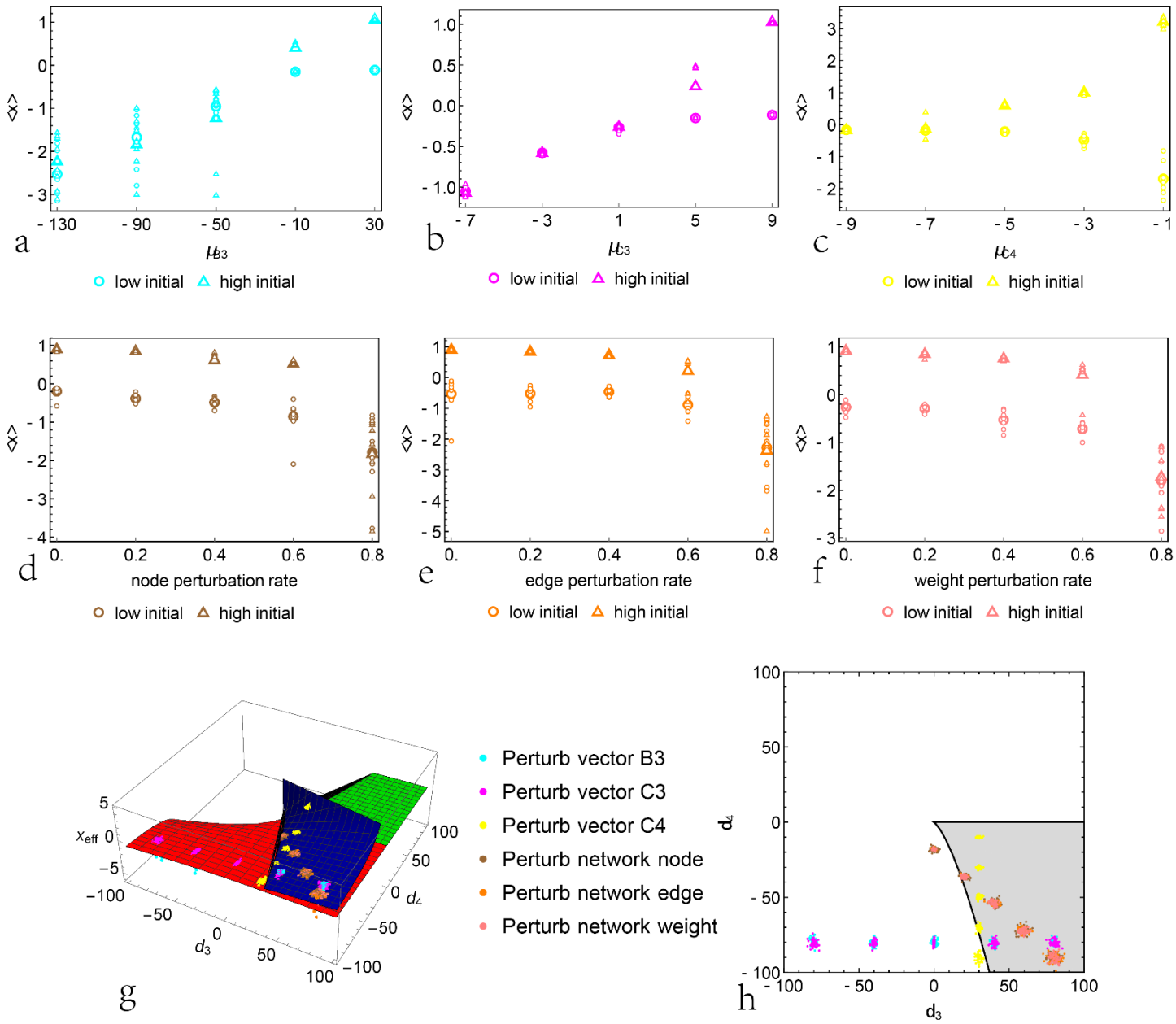

Figure S9. Changes in stable states shown in Fig. S8. Related to Fig. 1. *As a result of changes in (a) the mean* μ_{B^3} *of vector* B^3*; (b) the mean* μ_{C^3} *of vector* C^3*; (c) the mean* μ_{C^4} *of vector* C^4*; (d) the rate of removal of network nodes; (e) the rate of removal of network edges; (f) the rate of reduction of network weights. For each case, we run 50 simulations, and the large marker represents their average with different initial conditions. (g) Effective state of the system in three-dimensional space composed of the state variable* x_{eff} *and parameters* d_3, d_4*. Each colored surface represents one stable state in the manifold. The points representing the steady states in the complete multidimensional model as a function of changes in the parameters of the dynamics collapse onto the manifold. (h) The projection of (g) by eliminating the dimension* x_{eff}*. The gray region represents the bi-stable region, and the black curve represents the critical boundary.*

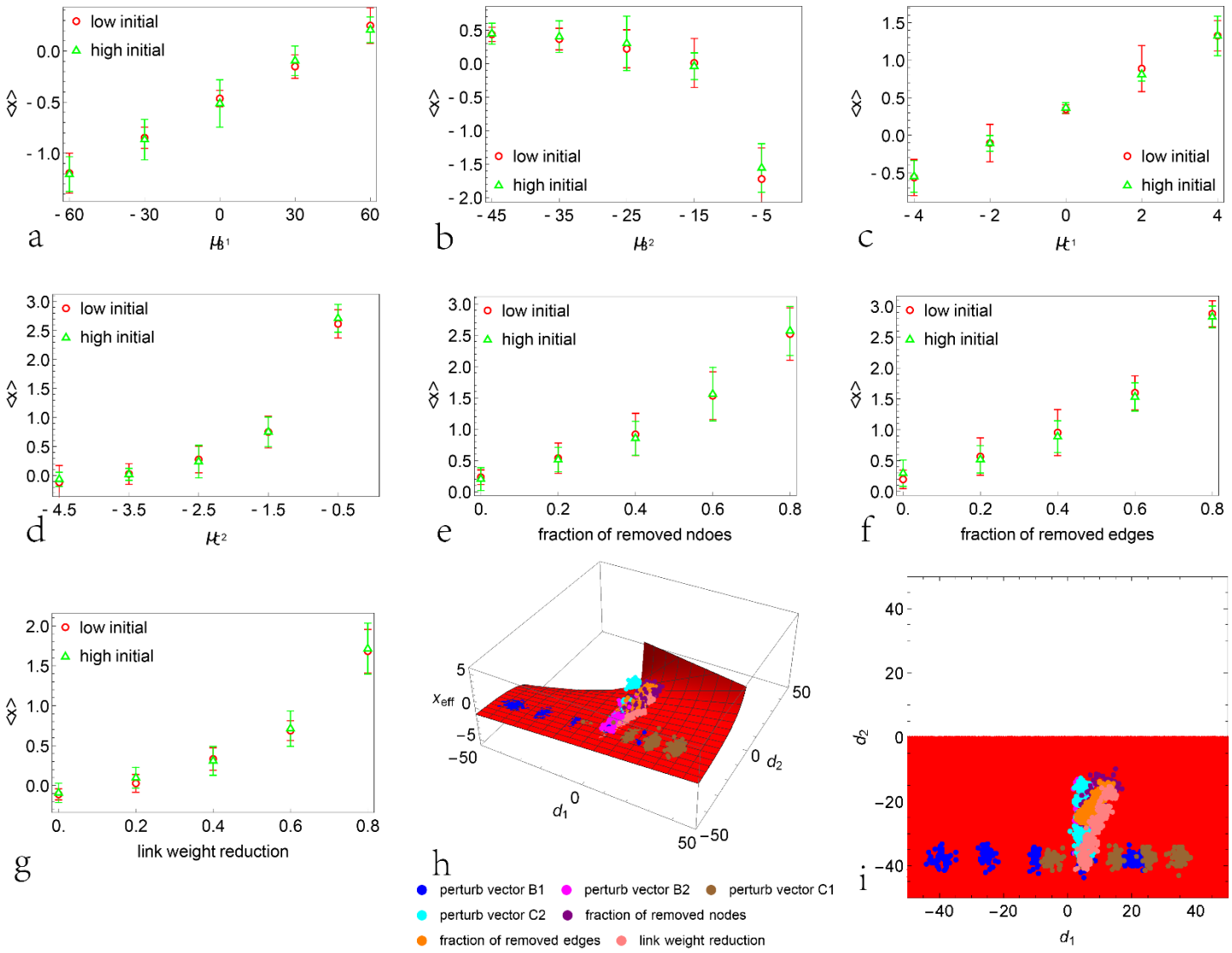

Figure S10. Results obtained from numerical simulation and theoretical predication as a function of changes on non-homogeneous dynamics. Related to Fig. 1. *Average state of the system as a function of changes in (a) the mean* μ_{B^1} *of vector* B^1*; (b) the mean* μ_{B^2} *of vector* B^2*; (c) the mean* μ_{C^1} *of vector* C^1*; (d) the mean* μ_{C^2} *of vector* C^2*; (e) the rate of removal of network nodes; (f) the rate of removal of network edges; (g) the rate of reduction of network weights. For each case, we run 50 simulations and the error bar represents its mean and one standard deviation. (h) Effective state of the system in three-dimensional space composed of the state variable* x_{eff} *and effective parameters* d_1, d_2*. Each colored surface represents one stable state in the manifold. The points representing the steady states in the complete multidimensional model as a function of changes in the parameters of the dynamics collapse onto the manifold. (i) The projection of (h) by eliminating the dimension* x_{eff}*. The enlargement of marker points represents the increase of corresponding perturbation.*

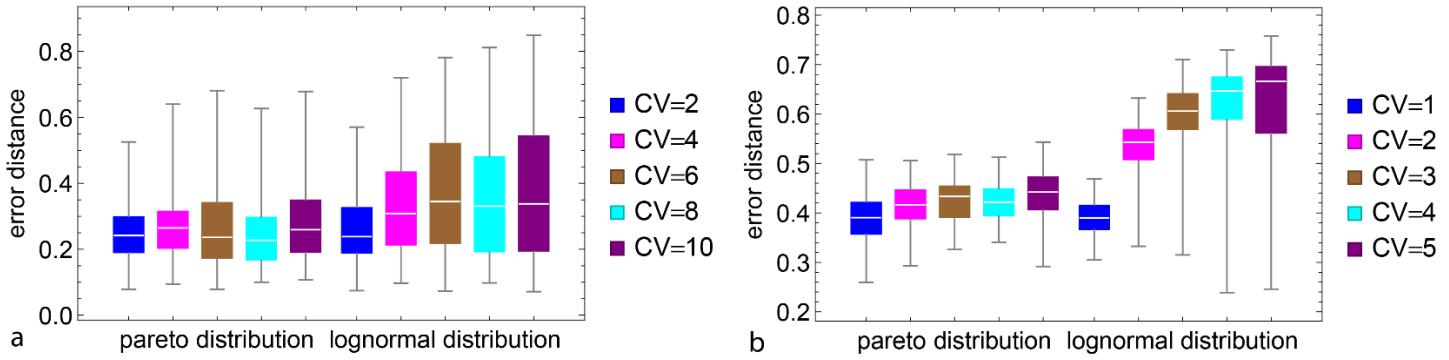

Figure S11. Comparison of error distance of SIS model with vector $\mathbf{e}$ from a pareto and lognormal distribution with fixed mean and varying the CV. Related to Fig. 1. *Their mean is in (a) $\mu_e = 30$ and in (b) $\mu_e = 70$.*

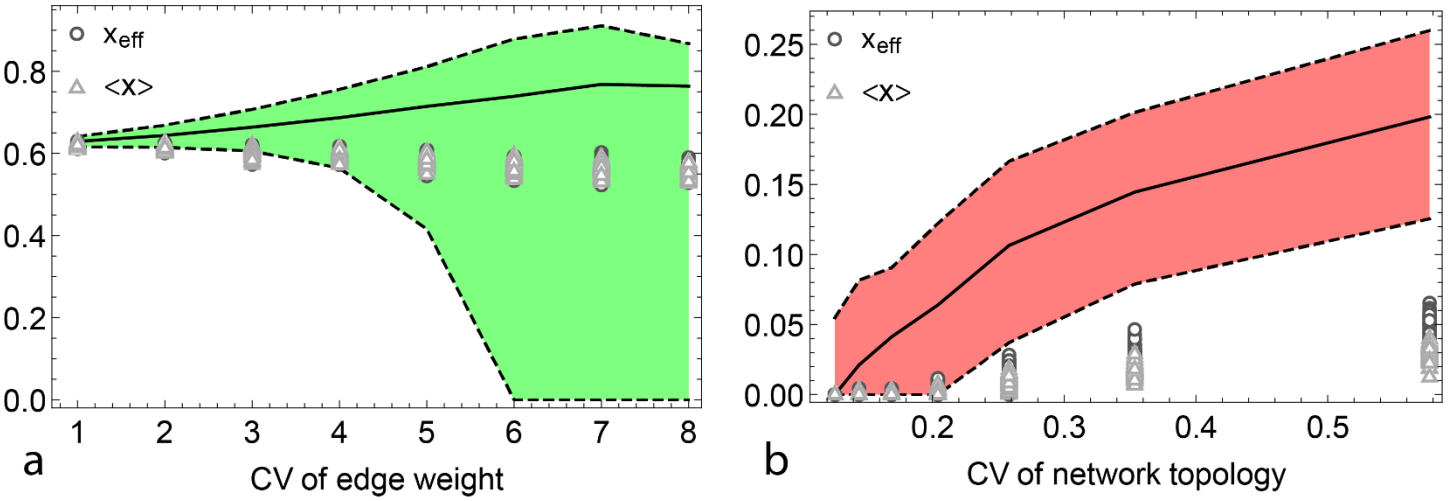

Figure S12. Results obtained from numerical simulation and theoretical predication as a function of changes on epidemic dynamics with strong heterogeneity. Related to Fig. 1. *The solution of the epidemic dynamics as a function of changes in (a) CV of lognormal distribution of edge weight ranging from 1 to 8 (and topology is generated by ER network with connectivity 0.4); (b) CV of degree distribution in which scale parameter α of degree distribution $P(k) \sim k^{-\alpha}$ ranging from 4 to 10. The vector $\mathbf{e} = (e_1, \ldots, e_N)^T$ are constant 30. In each panel, the solid black line is obtained by averaging the analytical prediction $< x^*_{eff}(d_2, d_3) >$ over 50 realizations of matrix $\mathbf{A}$ and vector $\mathbf{e}$ through $d_2(e_{eff}, A_{eff})$ and $d_3(A_{eff})$. The dashed line represents the corresponding confidence level of three standard deviations.*

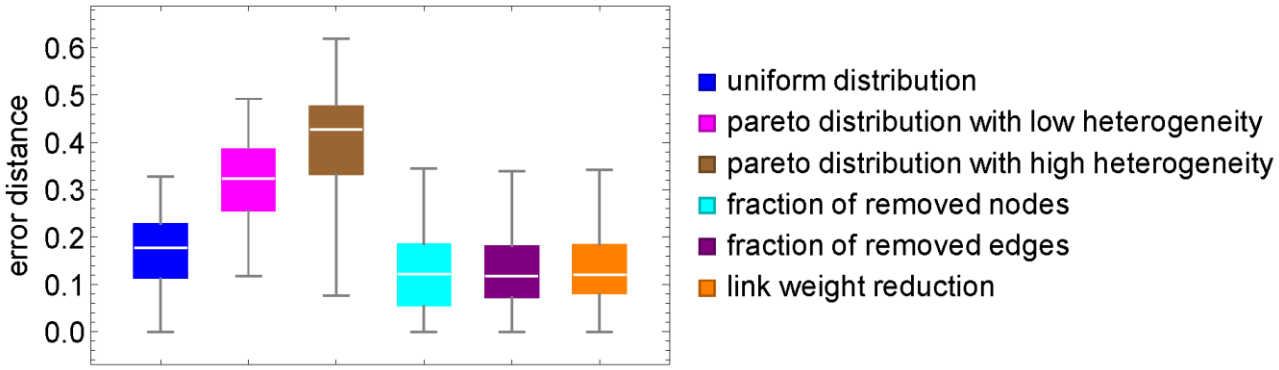

Figure S13. Error distance $err_x = \left| x_{eff} - x(d_1,\ldots,d_S) \right|$ **for the epidemic dynamics. Related to Fig. 1.** *The network* $\mathbf{A}$ *is given by the empirical data(Isella et al., 2011, Rossi and Ahmed, 2015), while the recovery rates* $\mathbf{e} = (e_1,\ldots,e_N)^T$ *are random parameters drawn from: a) uniform distribution (in blue) between 0 and* $2\mu_e$*, where* μ_e *ranges from 30 to 70 with interval of 10; b) Pareto type II distribution* $P(x) = \left(1 + \frac{x-\mu}{k}\right)^{-\alpha}$, $x > \mu$ *with low heterogeneity (in magenta), with* k *ranging from 270 to 630 with interval 90, fixed shape parameter* $\alpha = 10$*, and location parameter* $\mu = 0$ *to guarantee the same change of mean as uniform distribution. c) Pareto distribution with high heterogeneity (in brown) with* k *ranging from 33 to 77 with interval 11, fixed shape parameter* $\alpha = 2.1$*, and location parameter* $\mu = 0$*; d) after different types of perturbations (see color legend) and recovery rates* $\mathbf{e} = (e_1,\ldots,e_N)^T$ *distributed uniformly between 0 and* $2\mu_e$ *where* μ_e *= 30.*

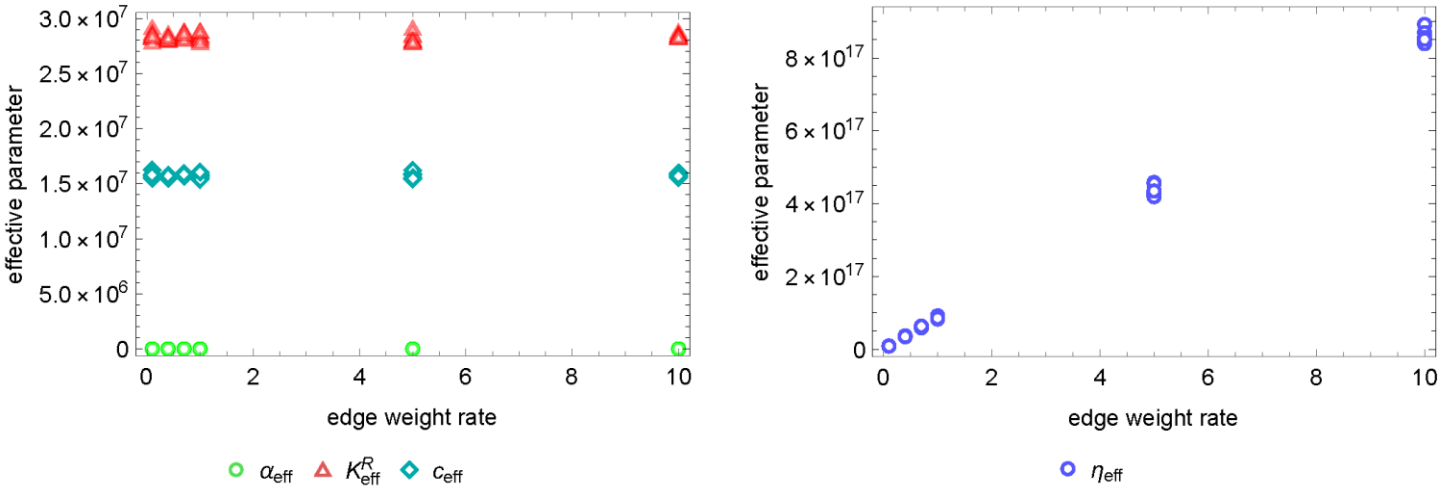

Figure S14. Parameters changes as a result of reduction in edge weights. Related to Fig. 3. *Changes in (a)* $\alpha_{eff}, K^R_{eff}, c_{eff}$ *and (b)* η_{eff} *as a function of the trade weight reduction factor,* $f_w = 0.1, 0.4, 0.7, 1, 5, 10$.

Transparent Methods

1. Previous work and relation of resilience of complex systems

1.1. Classic one-dimensional method to quantify resilience

We start by presenting the traditional mathematical method (Lyapunov, 1992) to evaluate the resilience in a one-dimensional system driven by the nonlinear dynamic equation

$$\frac{dx}{dt} = f(\beta, x) \quad (1)$$

where $f(\beta, x)$ represents the system's dynamics and β is the control parameter to capture the variable conditions. If for a stable fixed point x^* of Eq. (1), the following conditions hold:

$$\begin{cases} f(\beta, x^*) = 0 \\ \lambda = \dfrac{\partial f}{\partial x}|_{x=x^*} < 0 \end{cases} \quad (2)$$

then, the solution of these conditions is called the stability domain for x^*.

$$x^*(\beta). \quad (3)$$

Eq. (2) guarantees that the system is in its steady state and that it is linearly stable around the steady state; i.e., for small perturbations, the system will return to the unperturbed equilibrium point x^*. In this case, Eq. (3) represents the possible stable states x^* of the system as a function of the control parameter β.

The shape of the $x^*(\beta)$ is given by Eq. (3) and is uniquely determined by the functional form of $f(\beta, x)$. If this function exhibits a fold-type bifurcation (Fig. S1), then either one of three equilibria may exist, depending on the value of the control parameter β. The colored lines in the $\beta - x$ plane represent the equilibrium solutions, i.e., the values $x^*(\beta)$ such that $f(\beta, x^*) = 0$. The black arrows indicate the direction in which the system moves if it is not in equilibrium. It can be seen from these arrows that all curves represent stable equilibria except for the blue middle curve (unstable state). If the system is the lower stable state (Fig. S1, red line) as β is increases, no major change is observed in the state of the system until β reaches a critical value, β_c. Although no big changes occur in the stable states, its resilience decreases because smaller and smaller perturbations are needed to determine the shift to the stability domain of the other attractor (green line). At the critical point β_c of Eq. (3) the system of Eq. (1) undergoes a transition to the other stable state. This is known as a critical transition and is a well-studied phenomenon in the complex system literature (Stanley, 1999, Sornette, 2006, Dorogovtsev et al., 2008, Scheffer et al., 2012, Suweis and D'Odorico, 2014).

Therefore, in the one-dimensional equation (1), a complete analytical treatment of the resilience of the system is possible (Lyapunov, 1992). We can identify the critical value of the control parameter β and study the effect of external perturbations on the system. Recently, a number of studies have investigated how to anticipate or avoid critical transitions in the system. The classic one-dimensional method (Lyapunov, 1992) presented above assumes that the system dynamics can be approximated by a one-dimensional equation, Eq. (1), where β represents the endogenous effects on the system. Although this method is conceptually powerful, it has very limited applicability to "real-world" problems, as it is unable to account for the resilience of complex high-dimensional systems.

1.2. Critical slowing down

One of the most commonly used leading indicators of critical transitions is provided by the phenomenon of critical slowing down (CSD). In dynamical systems, the phenomenon of CSD is indeed a good indicator that the system is approaching a critical threshold (Wissel, 1984). For example, in Fig. S1, if the system approaches the fold bifurcation point β_c, the dominant eigenvalue characterizing the rates of change of x around the equilibrium becomes zero, and consequently, the recovery rates decrease smoothly to zero (Van Nes and Scheffer, 2007, Scheffer et al., 2009, Scheffer et al., 2012). CSD tends to lead to an increase in the value of AR1 (Ives, 1995) (lag-1 autocorrelation) and the variance (Carpenter and Brock, 2006) of the fluctuations in a stochastically forced system approaching a bifurcation for a critical value of the control parameter.

For simplicity, let us consider the one-dimensional system given by Eq. (1) for discrete time steps, and let us call x^* its equilibrium at stationarity. If we assume the system is perturbed around x^* and we quantify the deviation of the state variable x from the equilibrium at time step n as $y_n = x_n - x^*$, then we can describe the dynamic of y_n by linearizing the dynamic around x^*, i.e. $y_{n+1} = y_n + \lambda y_n$. Then, after a period Δt, we have that $y_{n+1} = e^{\lambda \Delta t} y_n$, i.e., the return to equilibrium is exponential with a certain recovery speed λ. If we add Gaussian noise mimicking continuous perturbation of the stationary solution, then the previous equation becomes $y_{n+1} = e^{\lambda \Delta t} y_n + \sigma \epsilon_n$, where ϵ_n is a random number chosen from a standard normal distribution and σ is the standard deviation. If λ and Δt are independent of y_n, this model is a first-order autoregressive process $y_{n+1} = \alpha y_n + \sigma \epsilon_n$ where $\alpha = e^{\lambda \Delta t}$ is the autocorrelation. The expectation and standard deviation of the classic first-order autoregressive process $y_{n+1} = c + \alpha y_n + \sigma \epsilon_n$ are $E(y_{n+1}) = E(c) + \alpha E(y_n) + E(\sigma \epsilon_n) \Rightarrow \mu = c + \alpha \mu + O \Rightarrow \mu = \frac{c}{1-\alpha}$ and $Var(y_{n+1}) = E(y_{n+1}^2) - \mu^2 = \frac{\sigma^2}{1-\alpha^2}$. When the system approaches the critical point, the speed of the return to equilibrium decreases (λ approaches zero), the autocorrelation α tends toward one and the variance tends toward infinity.

In sum, in the dynamics of a system approaching a bifurcation, CSD leads to (i) slower recovery from perturbations, (ii) increased autocorrelation and (iii) increased variance. All these indicators can be used to detect early warning signs of critical transitions (Scheffer et al., 2009).

The CSD method could in theory inform us about the fact that a high-dimensional complex system is approaching the critical point, it also has many limitations, such as the difficult-to-control sensitivity of the system parameters and the high (exponentially increasing) computational costs of investigating the critical transition for several combinations of the system parameters. Additionally, it does not provide testable predictions of the system's response to different perturbations, and it does not give insights that allow for the design or optimization of the resilience of high-dimensional systems.

1.3. One-dimensional effective equation

Gao *et al*.(Gao et al., 2016) developed a method that can predict and explore the resilience of network-based dynamical systems and provided a new way to understand the resilience of complex natural and human-made systems. These authors consider a class of equations describing the dynamics of several types of high-dimensional systems with pairwise interactions:

$$\frac{dx_i}{dt} = F(x_i) + \sum_{j=1}^{N} A_{ij} G(x_i, x_j) \quad (4)$$

where $\mathbf{x} = (x_1, ..., x_N)$ is the set of activities of the components/nodes of N and the functions $F(x_i)$ and $G(x_i, x_j)$ represent the self-dynamics and coupling dynamics and these functions are the same at all nodes. Finally, the weight matrix A_{ij} specifies the interactions between nodes.

Analogous to the classic one-dimensional method, a transition from a desired to an undesired stable state captures the loss of resilience in a high-dimensional networked system. The key difference is that Eq. (4) is not controlled by only one parameter (e.g., β in Eq. (1)); rather, it depends on the matrix A_{ij}, which is composed of N^2 parameters. Therefore, resilience loss can be induced by changes in any of the N^2 parameters. For instance, the extinction of species in an ecological system may correspond to the removal of one or several nodes (Gao et al., 2016). Therefore, the resilience function of a networked system is a high-dimensional manifold over the parameter space characterizing the system. This framework requires the dynamics to be the same at all nodes; i.e., the self-dynamics and coupling dynamics of all nodes are the same. Therefore, many processes such as the generalized Lotka-Volterra dynamics that are frequently used to describe ecologic systems, cannot be investigated with this framework. In fact, it is rare that the self-dynamics and coupling dynamics of different nodes are the same.

1.4. Dimension reduction based on spectral graph theory

Recently, Laurence *et al.*(Laurence et al., 2019) considered the same class of equations as Gao *et al*.(Gao et al., 2016) and developed a polynomial approximation to reduce complex networks using the spectral graph theory. The activity of the reduced systems is used as an indicator of the global activity of large networks and the dominant eigenvectors of the adjacency matrix are central to the global states' evolution. Let's consider Eq. (4); the procedure to apply this one-dimensional reduction is as follows: (i) compute the dominant eigenvalue α and the corresponding eigenvector $\mathbf{v}$ of the transposed of the adjacency matrix $\mathbf{A}$; (ii) define the normalized eigenvector $\mathbf{a} = \mathbf{v} / (\mathbf{1}^T \mathbf{v})$ and obtain the structural parameter $\beta = \frac{1}{\alpha} \frac{\mathbf{a}^T \mathbf{K} \mathbf{a}}{\mathbf{a}^T \mathbf{a}}$ where $\mathbf{K}$ is a diagonal matrix with diagonal elements $K_{ii} = \sum_{j=1}^{N} A_{ij}$; (iii) the one-dimensional equation is $\frac{dx_{eff}}{dt} = F(x_{eff}) + \alpha G(\beta x_{eff}, x_{eff})$ where $x_{eff} = \mathbf{a}^T \mathbf{x}$. This method can adopt more eigenvalues and be extended to modular, heterogeneous, and bipartite networks, etc. analytically. Pan *et al.*(Pan et al., 2020) developed a theory for interacting spreading dynamics on complex networks. Thibeault *et al.*(Thibeault et al., 2020) proposed a Dynamics Approximate Reduction Technique that maps high-dimensional dynamics to low-dimensional dynamics to predict the impact of network topology and dynamics on synchronization.

Analogous to Gao *et al*.(Gao et al., 2016), Laurence *et al.*(Laurence et al., 2019) tackle the same problem of reducing high-dimensional networked systems (with the same self-dynamics and coupling-dynamics at all nodes) to one-dimensional effective system. Further, they show that the proposed reduction of Gao *et al.*(Gao et al., 2016) is a special case of the general scheme when applied to uncorrelated random networks. Finally, this approach has the same limitation as Gao *et al.*'s framework because it does not allow the self-dynamics and coupling dynamics to change from node to node, thereby impeding the application to a variety of "real-world" cases.

2. Framework of dimensional reduction

2.1. Reduce high-dimensional equations

As given by Eq. 1 of main text, the dynamics of each node depend on the node itself (given by the "self-dynamics" $F_i(x_i)$) and on the interaction with its nearest neighbors (given by the interaction network and coupling dynamics $\sum_{j=1}^{N} A_{ij} G_i(x_i, x_j)$). Therefore, the dynamics of the average nearest-neighbor nodes represent an important contribution to the overall system's dynamics. To quantify this contribution, we define an operator $\mathcal{L}(\mathbf{x}) = \frac{1}{N} \sum_{j=1}^{N} s_j^{out} x_j \Big/ \frac{1}{N} \sum_{j=1}^{N} s_j^{out} = \frac{\langle \mathbf{s}^{out} . \mathbf{x} \rangle}{\langle \mathbf{s}^{out} \rangle}$, where $\mathbf{s}^{out} = (s_1^{out}, \ldots, s_N^{out})$ is the vector of the out-degree of the interaction network $\mathbf{A}$ (Gao et al., 2016). The operator $\mathcal{L}$ is feasible for a linear time-invariant (LTI) function; i.e., the following equation holds:

$$\mathcal{L}(a\mathbf{x}+b\mathbf{y}) = a\mathcal{L}(\mathbf{x}) + b\mathcal{L}(\mathbf{y}) \quad (5)$$

where $\mathbf{x}$ and $\mathbf{y}$ are vectors and a and b are constants. If vectors $\mathbf{x}$ and $\mathbf{y}$ are weakly correlated, we can obtain

$$\mathcal{L}(\mathbf{x}\circ\mathbf{y}) \approx \mathcal{L}(\mathbf{x})\mathcal{L}(\mathbf{y}) \quad (6)$$

where $\circ$ is the Hadamard product such that $\mathbf{x}\circ\mathbf{y} = \left(x_1 y_1, \cdots, x_N y_N\right)^T$ (see Transparent Methods, section Validation of the Hadamard product).

If the degree correlation of network $\mathbf{A}$ is weak (the neighborhood of node i is similar to the neighborhoods of all other nodes), then $\sum_j^N A_{i,j} G_i(x_i, x_j) \approx s_i^{in} \mathcal{L}(G_i(x_i, \mathbf{x}))$. Furthermore, if $G_i(x_i, x_j)$ is linear in x_j or the standard deviation in the elements of the vector $\mathbf{x}$ is small, then $\mathcal{L}(G_i(x_i, \mathbf{x})) \approx G_i(x_i, \mathcal{L}(\mathbf{x})) = G_i(x_i, x_{eff})$, where $x_{eff} = \mathcal{L}(\mathbf{x})$. Therefore, Eq. (1) in the main text can be written as $\frac{dx_i}{dt} \approx F_i(x_i) + s_i^{in} G_i(x_i, x_{eff})$, and its vector notation is

$$\frac{d\mathbf{x}}{dt} = \mathbf{F}(\mathbf{x}) + \mathbf{s}^{in} \circ \mathbf{G}(\mathbf{x}, x_{eff}) \quad (7)$$

where the vector function $\mathbf{F}(\mathbf{x}) = \left(F_1(x_1), \ldots, F_N(x_N)\right)^T$ and $\mathbf{G}(\mathbf{x}, x_{eff}) = \left(G_1(x_1, x_{eff}), \ldots, G_N(x_N, x_{eff})\right)^T$.

If each $F_i(x_i)$ is a linear combination of m subfunctions, i.e., $F_i(x_i) = b_{i,1} f_1(x_i) + b_{i,2} f_2(x_i) + \cdots + b_{i,m} f_m(x_i)$, then according to Eq. (5), $\mathcal{L}(\mathbf{F}(\mathbf{x})) = \mathcal{L}\begin{pmatrix} F_1(x_1) \\ \vdots \\ F_N(x_N) \end{pmatrix} = \mathcal{L}\begin{pmatrix} b_{1,1} f_1(x_1) \\ \vdots \\ b_{N,1} f_1(x_N) \end{pmatrix} + \ldots + \mathcal{L}\begin{pmatrix} b_{1,m} f_m(x_1) \\ \vdots \\ b_{N,m} f_m(x_N) \end{pmatrix}$. According to Eq. (6),

$$\begin{aligned} \mathcal{L}(\mathbf{F}(\mathbf{x})) &= \mathcal{L}(B^1 \circ f_1(\mathbf{x})) + \cdots + \mathcal{L}(B^m \circ f_m(\mathbf{x})) \\ &\approx \mathcal{L}(B^1)\mathcal{L}(f_1(\mathbf{x})) + \cdots + \mathcal{L}(B^m)\mathcal{L}(f_m(\mathbf{x})) \end{aligned},$$

where $B^k = \left(b_{1,k}, \ldots, b_{N,k}\right)^T$ is the k-th column of matrix B. Because the node dynamics are uniform,

$$\begin{aligned} \mathcal{L}(\mathbf{F}(\mathbf{x})) &\approx \mathcal{L}(B^1) f_1(\mathcal{L}(\mathbf{x})) + \ldots + \mathcal{L}(B^m) f_m(\mathcal{L}(\mathbf{x})) \\ &\approx \mathcal{L}(B^1) f_1(x_{eff}) + \ldots + \mathcal{L}(B^m) f_m(x_{eff}) \\ &= \sum_{k=1}^{m} \mathcal{L}(B^k) f_k(x_{eff}) \end{aligned} .$$

Similarly, if each $G_i(x_i, x_j)$ is a linear combination of n subfunctions, i.e., $G_i(x_i, x_j) = c_{i,1} g_1(x_i, x_j) + \cdots + c_{i,n} g_n(x_i, x_j)$, then

$$\begin{aligned}\mathcal{L}(\mathbf{G}(\mathbf{x}, x_{eff})) &\approx \mathcal{L}(C^1)g_1(x_{eff}, x_{eff}) + \ldots + \mathcal{L}(C^n)g_n(x_{eff}, x_{eff}) \\ &= \sum_{l=1}^{n} \mathcal{L}(C^l)g_l(x_{eff}, x_{eff})\end{aligned} \quad ,$$

where $C^l = \left(c_{1,l}, \ldots, c_{N,l}\right)^T$ is the l-th column of matrix C.

We apply the operator $\mathcal{L}$ to both sides of Eq. (7), in vector notation, and obtain

$$\begin{aligned}\frac{d\mathcal{L}(\mathbf{x})}{dt} &= \mathcal{L}(\mathbf{F}(\mathbf{x}) + \mathbf{s}^{in} \circ \mathbf{G}(\mathbf{x}, \mathcal{L}(\mathbf{x}))) \\ &\approx \mathcal{L}(\mathbf{F}(\mathbf{x})) + \mathcal{L}(\mathbf{s}^{in})\mathcal{L}(\mathbf{G}(\mathbf{x}, \mathcal{L}(\mathbf{x}))) \\ &\approx \sum_{k=1}^{m} \mathcal{L}(B^k) f_k(x_{eff}) + \mathcal{L}(\mathbf{s}^{in}) \sum_{l=1}^{n} \mathcal{L}(C^l) g_l(x_{eff}, x_{eff})\end{aligned} \quad .$$

Finally, we obtain the effective equation

$$\frac{dx_{eff}}{dt} \approx \sum_{k=1}^{m} B_{eff}^k f_k(x_{eff}) + A_{eff} \sum_{l=1}^{n} C_{eff}^l g_l(x_{eff}, x_{eff}) \text{ , (8)}$$

where $A_{eff} = \mathcal{L}(\mathbf{s}^{in})$, $B_{eff}^k = \mathcal{L}(B^k)$, and $C_{eff}^l = \mathcal{L}(C^l)$.

2.2. Self-dynamics and coupling-dynamics are polynomials

If $F_i(x_i)$ is not a linear combination of m subfunctions or if $F_i(x_i)$ varies from node to node (i.e., it is different for different nodes i), we can use Chebyshev polynomials to approximate it (see Transparent Methods, sections Chebyshev approximation theory and Validation of the Chebyshev approximation), minimizing the error between $F_i(x_i)$ and $\sum_{k=1}^{m} b_{i,k} x^{(k-1)}$. Therefore, $F_i(x_{eff}) = \sum_{k=1}^{m} b_{i,k} x_{eff}^{(k-1)}$. Similarly, we can substitute $G_i(x_i, x_j)$ for $\sum_{p,q=1}^{n/2} d_{p,q} x_i^{(p-1)} x_j^{(q-1)}$. Therefore, $G_i(x_{eff}, x_{eff}) = \sum_{l=1}^{n} c_{i,l} x_{eff}^{(l-1)}$, where $c_{i,l}$ collects all terms $d_{p,q}$ such that $l = p + q - 1$. Therefore, the final effective equation is

$$\frac{dx_{eff}}{dt} \approx \sum_{k=1}^{m} B_{eff}^k x_{eff}^{(k-1)} + A_{eff} \sum_{l=1}^{n} C_{eff}^l x_{eff}^{(l-1)} \quad (9)$$

Eq. (9) has $m + n + 2$ variables: $A_{eff}, x_{eff}, B_{eff}^k, C_{eff}^l$, where $k = 1, \ldots, m; l = 1, \ldots, n$. To further decrease the number of variables, Eq. (9) can be written as

$$\frac{dx_{eff}}{dt} \approx \begin{cases} \sum_{k=1}^{m} (B_{eff}^{k} + A_{eff} * C_{eff}^{k}) x_{eff}^{(k-1)} + \sum_{l=m+1}^{n} A_{eff} C_{eff}^{l} x_{eff}^{(l-1)}, n \geq m \\ \sum_{l=1}^{n} (B_{eff}^{l} + A_{eff} * C_{eff}^{l}) x_{eff}^{(l-1)} + \sum_{k=n+1}^{m} B_{eff}^{k} x_{eff}^{(k-1)}, n \leq m \end{cases}$$

Finally, we obtain

$$I(d_1, \ldots, d_S, x_{eff}) = \frac{dx_{eff}}{dt} \approx \sum_{s=1}^{S} d_s * x_{eff}^{s-1} \quad (10)$$

where $S = \max(m, n)$ and $d_s = \begin{cases} B_{eff}^{s} + A_{eff} * C_{eff}^{s}, s \in [1, \min(m, n)] \\ A_{eff} C_{eff}^{s}, s \in [m+1, n], m < n \\ B_{eff}^{s}, s \in [n+1, m], n < m \end{cases}$. This reduction maps the equation of the high-dimensional networked system, Eq. 1 of main text, into a low-dimensional effective equation with $\max(n, m)$ parameters and the state variable x_{eff}.

3. Chebyshev approximation theory

Based on approximation theory, mathematically, Chebyshev polynomials provide an efficient way to approximate a smooth nonperiodic function (Boyd, 2001, Mason and Handscomb, 2002). Specifically, Chebyshev polynomials, named after Pafnuty Chebyshev (Chebyshev, 1853), are a sequence of orthogonal polynomials that are related to de Moivre's formula and can be defined recursively. Chebyshev polynomials are important in approximation theory because the roots of the Chebyshev polynomials of the first kind, which are also called Chebyshev nodes, are used as nodes in polynomial interpolation. The resulting interpolation polynomial minimizes the problem of Runge's phenomenon and provides an approximation that is close to the polynomial that best approximates a continuous function under the maximum norm.

Chebyshev polynomials of the first kind can be defined as the unique polynomials satisfying $T_n(\cos\theta) = \cos(n\theta)$, and their recurrence relation is $T_0(x) = 1, T_1(x) = x, T_{n+1}(x) = 2xT_n(x) - T_{n-1}(x)$. They are polynomials with the largest possible leading coefficient, subject to the condition that the interval is $[-1,1]$, and they satisfy the orthogonality relation $\int_{-1}^{1} T_m(x) T_n(x) (1-x^2)^{-1/2} dx = 0$, where $n \neq m$. Because the set of Chebyshev polynomials form an orthonormal basis, a function in the same space on $-1 \leq x \leq 1$ can be expressed via the expansion $f(x) = \sum_{n=0}^{\infty} a_n T_n(x)$, where a_n is called the Chebyshev coefficient, and this sum is called a Chebyshev series. As long as the function f is continuous and at least somewhat smooth (Lipschitz continuity is sufficient), it has a unique expansion of this form that converges absolutely and

uniformly, the coefficients of which are given by the integral $a_n = \frac{2}{\pi}\int_{-1}^{1} \frac{f(x)T_n(x)}{\sqrt{1-x^2}}dx$; for $n = 0$, the constant changes from $2/\pi$ to $1/\pi$. Although the standard method of approximating a function is to form the polynomial obtained by truncating its Chebyshev expansion, $f_N(x) = \sum_{n=0}^{N} a_n T_n(x)$, it is rarely worth computing the best (minimax) approximation (Pachón and Trefethen, 2009). Instead, for practical computations, it is simpler to construct the approximations via Chebyshev interpolants, which can also be regarded as finite series in Chebyshev polynomials for some coefficients c_n, $p_N(x) = \sum_{n=0}^{N} c_n T_n(x)$. This approximation is not optimal, but these coefficients are nearly optimal and much easier to compute than those of the Chebyshev expansion. Each coefficient c_n will converge to a_k as $N \to \infty$, neglecting the effects of rounding errors, which are very small in relative terms (Battles and Trefethen, 2004). When the given function has two variables $f(x, y)$, the formalism is similar to that above for one variable. By using iterative Gaussian elimination with complete pivoting to construct low rank approximations, the function is approximated to essentially machine precision (Townsend and Trefethen, 2013).

Here, we use the MATLAB toolbox Chebfun (Trefethen, 2013, Driscoll et al., 2014) to calculate the Chebyshev coefficients a_n. The implementation of Chebfun is based on the mathematical fact that smooth functions can be represented very efficiently by polynomial interpolation. In particular, it provides a simple environment in which to demonstrate the approximants. For the self-dynamics $F_i(x_i)$, we can construct a one-variable Chebyshev polynomial with the function 'chebfun' in the toolbox. For the coupling dynamics $G_i(x_i, x_j)$, we can construct a two-variable Chebyshev polynomial with the function 'chebfun2' in the toolbox. Additionally, if the interval of the given function is $[x_a, x_b]$ instead of the default $[-1,1]$, Chebfun will first calculate the Chebyshev coefficients and then rescale the Chebyshev polynomials by replacing x with $\frac{2}{x_b - x_a}(x - \frac{x_a + x_b}{2})$ automatically.

4. Testing the model approximation

The core of our framework lies in the derivation presented above, which allows us to reduce the high-dimensional networked system to a low-dimensional effective system. In addition to the mean-field approximation and the negligible degree correlation, the derivation is based on two additional conditions: (i) The Hadamard product is valid for a pair of vectors; i.e., $\mathcal{L}(\mathbf{x}\circ\mathbf{y}) \approx \mathcal{L}(\mathbf{x})\mathcal{L}(\mathbf{y})$. (ii) The Chebyshev approximation can be made.

4.1. Validation of the Hadamard product

If both vectors $\mathbf{x}$ and $\mathbf{y}$ are not uniform, the $\mathcal{L}$ operator of their Hadamard product approximates the product of their $\mathcal{L}$ operator. When they are constant vectors, this approximation becomes exact. As heterogeneity increases, the error will increase.

To further examine this condition, we explicitly test the approximation. Assume that the elements of the $\mathbf{x}$ vector are drawn from a distribution with mean μ_x and standard deviation σ_x and that the $\mathbf{y}$ vector is generated in a similar way . We calculate $\mathcal{L}(\mathbf{x}\circ\mathbf{y})$ and $\mathcal{L}(\mathbf{x})\mathcal{L}(\mathbf{y})$, respectively. Finally, we compare their relative error $\left|\frac{\mathcal{L}(\mathbf{x}\circ\mathbf{y})-\mathcal{L}(\mathbf{x})\mathcal{L}(\mathbf{y})}{\mathcal{L}(\mathbf{x}\circ\mathbf{y})}\right|$. Fig. S2 shows the result with different coefficients of variation of $\mathbf{x}$ and $\mathbf{y}$. Although vectors $\mathbf{x}$ and $\mathbf{y}$ are heterogeneous, the relative error is small. Therefore, this approximation holds.

4.2. Validation of the Chebyshev approximation

If either the self-dynamics $F_i(x_i)$ is not a linear combination of m subfunctions or the form of $F_i(x_i)$ is different for different i, we use the Chebyshev polynomial to approximate it. The resulting interpolation polynomial minimizes the problem of Runge's phenomenon and provides an approximation that is close to the polynomial that best approximates a continuous function under the maximum norm. Fig. S3 shows some simple examples of this approximation.

5. Extended validation

In the above sections, we showed analytically that by mapping a given high-dimensional networked system to an $S+1$-dimensional space, one obtains a low-dimensional effective equation $I(d_1,\ldots,d_S,x_{eff})$. In the Results section of the main text, we showed some real-world cases to reveal the advantages of our framework. To further validate this technique, we conduct a set of extensive numerical tests on elementary effective equations.

5.1. Case of d1, d2

We assume the self-dynamics $F_i(x_i)=b_{i,1}$ and coupling dynamics $G_i(x_i,x_j)=c_{i,1}+c_{i,2}x_i$. The high-dimensional equation is $\frac{dx_i}{dt}=b_{i,1}+\sum_j^N A_{i,j}(c_{i,1}+c_{i,2}x_i)$, and its low-dimensional effective equation is $\frac{dx_{eff}}{dt}=d_1x_{eff}^0+d_2x_{eff}^1$ where $x_{eff}=\mathcal{L}(\mathbf{x})$, $d_1=B_{eff}^1+A_{eff}C_{eff}^1$ and $d_2=A_{eff}C_{eff}^2$.

For testing and validation, we set the network size $N = 50$; $B^1 = \left(b_{1,1},\ldots,b_{N,1}\right)^T$ is a vector whose elements are drawn from a normal distribution with mean μ_{B^1} and standard deviation $\sigma_{B^1} = \left|\mu_{B^1}/3\right|$, $C^1 = \left(c_{1,1},\ldots,c_{N,1}\right)^T$ is a vector whose elements are drawn from a normal distribution with mean μ_{C^1} and standard deviation $\sigma_{C^1} = \left|\mu_{C^1}/3\right|$, $C^2 = \left(c_{1,2},\ldots,c_{N,2}\right)^T$ is a vector whose elements are drawn from a normal distribution with mean μ_{C^2} and standard deviation $\sigma_{C^2} = \left|\mu_{C^2}/3\right|$, and A is a complete network whose weights are drawn from a normal distribution with mean μ_A and standard deviation $\sigma_A = \left|\mu_A/3\right|$. We set $\mu_{B^1} = 15$, $\mu_{C^1} = -1$, $\mu_{C^2} = -2.5$, and $\mu_A = 0.2$, and we set two of initial conditions: a low initial condition $X = \left(x_1,\ldots,x_N\right)^T$, whose elements are drawn from a uniform distribution between 0 and 0.1, and a high initial condition $X = \left(x_1,\ldots,x_N\right)^T$, whose elements are drawn from a uniform distribution between 0.9 and 1. Fig. S4 shows the results of changing each of the following parameters one at a time: μ_{B^1}, μ_{C^1}, μ_{C^2}, the network nodes, the network edges and the network weights.

5.2. Case of d1 and d3

We assume the self-dynamics $F_i(x_i) = b_{i,1}$ and coupling dynamics $G_i(x_i, x_j) = c_{i,1} + c_{i,3}x_i x_j$. The high-dimensional equation is $\frac{dx_i}{dt} = b_{i,1} + \sum_j^N A_{i,j}(c_{i,1} + c_{i,3}x_i x_j)$, and its low-dimensional effective equation is $\frac{dx_{eff}}{dt} = d_1 x_{eff}^0 + d_3 x_{eff}^2$ where $x_{eff} = \mathcal{L}(\mathbf{x})$, $d_1 = B_{eff}^1 + A_{eff}C_{eff}^1$ and $d_3 = A_{eff}C_{eff}^3$.

For testing and validation, we set the network size $N = 50$; $B^1 = \left(b_{1,1},\ldots,b_{N,1}\right)^T$ is a vector whose elements are drawn from a normal distribution with mean μ_{B^1} and standard deviation $\sigma_{B^1} = \left|\mu_{B^1}/3\right|$, $C^1 = \left(c_{1,1},\ldots,c_{N,1}\right)^T$ is a vector whose elements are drawn from a normal distribution with mean μ_{C^1} and standard deviation $\sigma_{C^1} = \left|\mu_{C^1}/3\right|$, $C^3 = \left(c_{1,3},\ldots,c_{N,3}\right)^T$ is a vector whose elements are drawn from a normal distribution with mean μ_{C^3} and standard deviation $\sigma_{C^3} = \left|\mu_{C^3}/3\right|$, and A is a complete network whose weights are drawn from a normal distribution with μ_A and standard deviation $\sigma_A = \left|\mu_A/3\right|$. We set $\mu_{B^1} = -5$, $\mu_{C^1} = 3$, $\mu_{C^3} = -4$, and $\mu_A = 0.2$, and we set two initial conditions: a low initial value $X = \left(x_1,\ldots,x_N\right)^T$, whose elements are drawn from a uniform distribution between 0 and 0.1, and a high initial value $X = \left(x_1,\ldots,x_N\right)^T$, whose elements are drawn from a uniform distribution between 0.9 and 1.

Fig. S5 shows the results of changing one of the following parameters one at a time: μ_{B^1}, μ_{C^1}, μ_{C^3}, the network nodes, the network edges and the network weights.

5.3. Case of d2 and d3

We assume the self-dynamics $F_i(x_i) = b_{i,2}x_i$ and coupling dynamics $G_i(x_i, x_j) = c_{i,2}x_i + c_{i,3}x_i x_j$. The high-dimensional equation is $\frac{dx_i}{dt} = b_{i,2}x_i + \sum_j^N A_{i,j}(c_{i,2}x_i + c_{i,3}x_i x_j)$, and its low-dimensional effective equation is $\frac{dx_{eff}}{dt} = d_2 x_{eff}^1 + d_3 x_{eff}^2$ where $x_{eff} = \mathcal{L}(\mathbf{x})$, $d_2 = B_{eff}^2 + A_{eff}C_{eff}^2$ and $d_3 = A_{eff}C_{eff}^3$.

For testing and validation, we set the network size $N = 50$; $B^2 = \left(b_{1,2}, \ldots, b_{N,2}\right)^T$ is a vector whose elements are drawn from a normal distribution with mean μ_{B^2} and standard deviation $\sigma_{B^2} = \left|\mu_{B^2}/3\right|$, $C^2 = \left(c_{1,2}, \ldots, c_{N,2}\right)^T$ is a vector whose elements are drawn from a normal distribution with mean μ_{C^2} and standard deviation $\sigma_{C^2} = \left|\mu_{C^2}/3\right|$, $C^3 = \left(c_{1,3}, \ldots, c_{N,3}\right)^T$ is a vector whose elements are drawn from a normal distribution with mean μ_{C^3} and standard deviation $\sigma_{C^3} = \left|\mu_{C^3}/3\right|$, and A is a complete network whose weights are drawn from a normal distribution with μ_A and standard deviation $\sigma_A = \left|\mu_A/3\right|$. We set $\mu_{B^2} = -30$, $\mu_{C^2} = 5$, $\mu_{C^3} = -4$, and $\mu_A = 0.2$, and we set two initial conditions: a low initial value $X = \left(x_1, \ldots, x_N\right)^T$, whose elements are drawn from a uniform distribution between 0 and 0.1, and a high initial value $X = \left(x_1, \ldots, x_N\right)^T$, whose elements are drawn from a uniform distribution between 0.9 and 1. Fig. S6 shows the results of changing one of the following parameters one at a time: μ_{B^2}, μ_{C^2}, μ_{C^3}, the network nodes, the network edges and the network weights.

5.4. Case of d1, d2, and d3

We assume the self-dynamics $F_i(x_i) = b_{i,1} + b_{i,2}x_i$ and coupling dynamics $G_i(x_i, x_j) = c_{i,1} + c_{i,2}x_i + c_{i,3}x_i x_j$. The high-dimensional equation is $\frac{dx_i}{dt} = b_{i,1} + b_{i,2}x_i + \sum_j^N A_{i,j}(c_{i,1} + c_{i,2}x_i + c_{i,3}x_i x_j)$, and its low-dimensional effective equation is $\frac{dx_{eff}}{dt} = d_1 x_{eff}^0 + d_2 x_{eff}^1 + d_3 x_{eff}^2$ where $x_{eff} = \mathcal{L}(\mathbf{x})$, $d_1 = B_{eff}^1 + A_{eff}C_{eff}^1$, $d_2 = B_{eff}^2 + A_{eff}C_{eff}^2$ and $d_3 = A_{eff}C_{eff}^3$.

For testing and validation, we set the network size $N = 50$; $B^1 = \left(b_{1,1},\ldots,b_{N,1}\right)^T$ is a vector whose elements are drawn from a normal distribution with mean μ_{B^1} and standard deviation $\sigma_{B^1} = \left|\mu_{B^1}/3\right|$, $B^2 = \left(b_{1,2},\ldots,b_{N,2}\right)^T$ is a vector whose elements are drawn from a normal distribution with mean μ_{B^2} and standard deviation $\sigma_{B^2} = \left|\mu_{B^2}/3\right|$, $C^1 = \left(c_{1,1},\ldots,c_{N,1}\right)^T$ is a vector whose elements are drawn from a normal distribution with mean μ_{C^1} and standard deviation $\sigma_{C^1} = \left|\mu_{C^1}/3\right|$, $C^2 = \left(c_{1,2},\ldots,c_{N,2}\right)^T$ is a vector whose elements are drawn from a normal distribution with mean μ_{C^2} and standard deviation $\sigma_{C^2} = \left|\mu_{C^2}/3\right|$, $C^3 = \left(c_{1,3},\ldots,c_{N,3}\right)^T$ is a vector whose elements are drawn from a normal distribution with mean μ_{C^3} and standard deviation $\sigma_{C^3} = \left|\mu_{C^3}/3\right|$, and A is a complete network whose weights are drawn from a normal distribution with μ_A and standard deviation $\sigma_A = \left|\mu_A/3\right|$. We set $\mu_{B^1} = 12$, $\mu_{B^2} = -5$, $\mu_{C^1} = 0.25$, $\mu_{C^2} = 0.5$, $\mu_{C^3} = -1.5$, and $\mu_A = 0.2$, and we set two initial conditions: a low initial value $X = \left(x_1,\ldots,x_N\right)^T$, whose elements are drawn from a uniform distribution between 0 and 0.1, and a high initial value $X = \left(x_1,\ldots,x_N\right)^T$, whose elements are drawn from a uniform distribution between 0.9 and 1. Fig. S7 shows the results of changing one of the following parameters one at a time: μ_{B^1}, μ_{B^2}, μ_{C^1}, μ_{C^2}, μ_{C^3}, the network nodes, the network edges and the network weights.

5.5. Case of d1, d2, d3 and d4

We assume that the self-dynamics are $F_i(x_i) = b_{i,1}x_i^0 + b_{i,2}x_i^1 + b_{i,3}x_i^2$ and the coupling dynamics are $G_i(x_i, x_j) = c_{i,3}x_i x_j + c_{i,4}x_i^2 x_j$. Therefore, the high-dimensional equation is $\frac{dx_i}{dt} = b_{i,1}x_i^0 + b_{i,2}x_i^1 + b_{i,3}x_i^2 + \sum_j^N A_{ij}\left(c_{i,3}x_i x_j + c_{i,4}x_i^2 x_j\right)$. To conveniently represent resilience visually, we set $\forall i, b_{i,1} = -1, b_{i,2} = 1$ directly. In this way we can investigate the equilibrium states in a three-dimensional space. The high-dimensional equation becomes $\frac{dx_i}{dt} = -1 + x_i + b_{i,3}x_i^2 + \sum_j^N A_{i,j}(c_{i,3}x_i x_j + c_{i,4}x_i^2 x_j)$, and its low-dimensional effective equation is $\frac{dx_{eff}}{dt} = d_1 x_{eff}^0 + d_2 x_{eff}^1 + d_3 x_{eff}^2 + d_4 x_{eff}^3$ where $x_{eff} = \mathcal{L}(\mathbf{x})$, $d_1 = B_{eff}^1 = \mathcal{L}(B^1) = -1$, $d_2 = B_{eff}^2 = \mathcal{L}(B^2) = 1$, $d_3 = B_{eff}^3 + A_{eff}C_{eff}^3 = \mathcal{L}(B^3) + \mathcal{L}(\mathbf{s}^{in})\mathcal{L}(C^3)$ and $d_4 = A_{eff}C_{eff}^4 = \mathcal{L}(\mathbf{s}^{in})\mathcal{L}(C^4)$.

The predicted bifurcating resilience function is shown in Fig. S8, which has a transition from a resilient state with a single stable fixed point to a state with only limited resilience because of the presence of two stable fixed points. The critical boundary is fully determined by the polynomial $-1+x_{eff}+d_3x_{eff}^2+d_4x_{eff}^3$ with the two effective parameters d_3, d_4 on the macroscopic level, which depend on the elements of the interaction network A and the parameters of vectors B^3, C^3, C^4 on the microscopic level.

For testing and validation, we set the network size $N=50$; $B^3=\left(b_{1,3},\ldots,b_{N,3}\right)^T$ is a vector whose elements are drawn from a normal distribution with mean μ_{B^3} and standard deviation $\sigma_{B^3}=\left|\mu_{B^3}/3\right|$, $C^3=\left(c_{1,3},\ldots,c_{N,3}\right)^T$ is a vector whose elements are drawn from a normal distribution with mean μ_{C^3} and standard deviation $\sigma_{C^3}=\left|\mu_{C^3}/3\right|$, $C^4=\left(c_{1,4},\ldots,c_{N,4}\right)^T$ is a vector whose elements are drawn from a normal distribution with mean μ_{C^4} and standard deviation $\sigma_{C^4}=\left|\mu_{C^4}/3\right|$, and A is a complete network whose weights are drawn from a normal distribution with mean μ_A and standard deviation $\sigma_A=\left|\mu_A/3\right|$. We set $\mu_{B^3}=-10$, $\mu_{C^3}=5$, $\mu_{C^4}=-8$, and $\mu_A=0.2$, and we set two types of initial conditions: a low initial condition $X=\left(x_1,\ldots,x_N\right)^T$ whose elements are drawn from a uniform distribution between 0 and 0.1 and a high initial condition $X=\left(x_1,\ldots,x_N\right)^T$ whose elements are drawn from a uniform distribution between 0.9 and 1.

Fig. S9 a-f show the results of perturbing one of the following parameters at a time: μ_{B^3}, μ_{C^3}, μ_{C^4}, the network nodes, the network edges and the network weights. The low-dimensional effective equation predicts that the behavior observed in Fig. S9 a-f is, in fact, captured by a single effective function composed of three surfaces in a three-dimensional space d_3, d_4, x_{eff} (Fig. S9 g). Hence, we replot all the data of Fig. S9 a-f in this low-dimensional space, and we find that, as predicted, all data points collapse into the effective surfaces.

6. Non-homogeneous dynamics mechanisms

Our framework can be applied not only to non-homogeneous dynamic parameters where all nodes interact through the same mechanisms, especially when the parameter heterogeneity is large, but also to non-homogeneous dynamics mechanisms where the functional form of self-dynamics and coupling-dynamics differ across the nodes. Except for the example on gene expression shown in the main text, we here show a new illustrative example.

For testing and validation of non-homogeneous dynamics mechanisms, we assume the self-dynamics $F_i(x_i)=b_{i,1}$ if i is odd and $F_i(x_i)=b_{i,2}x_i$ if i is even, coupling dynamics $G_i(x_i,x_j)=c_{i,2}x_i$ if i is odd and $G_i(x_i,x_j)=c_{i,1}$ if i is even.

The high-dimensional equation is $\frac{dx_i}{dt} = b_{i,1} + \sum_j^N A_{i,j} c_{i,2} x_i$ if i is odd and $\frac{dx_i}{dt} = b_{i,2} x_i + \sum_j^N A_{i,j} c_{i,1}$ if i is even. Therefore, both self-dynamics and coupling dynamics are non-homogeneous. Its low-dimensional effective equation is $\frac{dx_{eff}}{dt} = d_1 + d_2 x_{eff}$ where $x_{eff} = \mathcal{L}(\mathbf{x})$, $d_2 = B_{eff}^2 + A_{eff} C_{eff}^2$ and $d_3 = A_{eff} C_{eff}^3$.

We set the network size $N = 50$; $B^1 = \left(b_{1,1}, \ldots, b_{N,1}\right)^T$ is a vector whose elements are drawn from a normal distribution with mean μ_{B^1} and standard deviation $\sigma_{B^1} = \left|\mu_{B^1} / 3\right|$, $B^2 = \left(b_{1,2}, \ldots, b_{N,2}\right)^T$ is a vector whose elements are drawn from a normal distribution with mean μ_{B^2} and standard deviation $\sigma_{B^2} = \left|\mu_{B^2} / 3\right|$, $C^1 = \left(c_{1,1}, \ldots, c_{N,1}\right)^T$ is a vector whose elements are drawn from a normal distribution with mean μ_{C^1} and standard deviation $\sigma_{C^1} = \left|\mu_{C^1} / 3\right|$, $C^2 = \left(c_{1,2}, \ldots, c_{N,2}\right)^T$ is a vector whose elements are drawn from a normal distribution with mean μ_{C^2} and standard deviation $\sigma_{C^2} = \left|\mu_{C^2} / 3\right|$, and A is a complete network whose weights are drawn from a normal distribution with mean μ_A and standard deviation $\sigma_A = \left|\mu_A / 3\right|$. We set $\mu_{B^1} = 30$, $\mu_{B_2} = -25$, $\mu_{C^1} = -2$, $\mu_{C^3} = -2.5$, and $\mu_A = 0.2$, and two of initial conditions: a low initial condition $X = \left(x_1, \ldots, x_N\right)^T$, whose elements are drawn from a uniform distribution between 0 and 0.1, and a high initial condition $X = \left(x_1, \ldots, x_N\right)^T$, whose elements are drawn from a uniform distribution between 0.9 and 1. Fig. S10 shows the results of changing each of the following parameters one at a time: μ_{B^1}, μ_{B^2}, μ_{C^1}, μ_{C^2}, the network nodes, the network edges and the network weights.

7. Effect of heterogeneity

7.1. Heterogeneity of self-dynamics

Our framework works for varied self-dynamics, especially for non-homogenous dynamics parameter even if its parameter distribution is heterogeneous. To prove this point, we present an analysis of the error distance distribution as displayed by the box whisker boxes, in the case of SIS dynamics with parameters $e_1, e_2, \ldots, e_N$ drawn from a Pareto or Log-normal distributions with different degree of heterogeneity. As it can be shown (see Fig. S11), although the extreme statistical values increase for increasing coefficient of variations of the distributions, the average error is quite stable across different CV. The error distance also depends the location of the average value of $\mathbf{e}$, i.e. when $\mu_e = 30$, $x_{eff} = 0$ (we are in the depleted state), while when $\mu_e = 70$, $x_{eff} > 0$ (we are in the sustainable state). We note that of course in the latter case, the variability is larger, and the effect of increasing CV is stronger, leading to larger errors.

7.2 Heterogeneity of network A

Our framework also works for high-dimensional networked system with heterogeneous network. For testing and validation, we adopt the SIS case from main text where network $\mathbf{A}$ is generated by random network model to test: (a) heterogeneity of edge weight. We generate one ER network with connectivity 0.4 and each edge weight is drawn from a lognormal distribution with mean 1 and CV from 1 to 8. (b) heterogeneity of network topology. We use Price graph model to generate random network whose degree distribution is $P(k) \sim k^{-\alpha}$ where α from 4 to 10 (Their corresponding CV of degree distribution are 0.57735, 0.353553, 0.258199, 0.204124, 0.169031, 0.144338, 0.125988). We set network size $N = 200$ and elements of vector $\mathbf{e} = (e_1, \ldots, e_N)^T$ are constant 30 (for better uncovering the effect of heterogeneity of network) and two initial conditions: a low initial value $X = (x_1, \ldots, x_N)^T$, whose elements are drawn from a uniform distribution between 0 and 0.1, and a high initial value $X = (x_1, \ldots, x_N)^T$, whose elements are drawn from a uniform distribution between 0.9 and 1. We find that the error between analytical solutions and numerical solutions increases as increasing network heterogeneity, including the heterogeneous of edge weight and heterogeneous of networks topology (see Fig. S12).

7.3 Heterogeneity of perturbations

Last, we show an additional example to show to what extent the error of our approximation may be acceptable, i.e. its performance is sufficiently good; we also show when our framework may not be valid if the dynamics are "too" heterogeneous, i.e. error may increase with increasing heterogeneity. In Fig. S13, we can see that the error distance depends both on the interaction network and on properties of the self-dynamics and the coupling-dynamics. In other words, it is not possible to disentangle the contribution of the network structure and of the dynamics to the error function.

Supplemental References

BATTLES, Z. & TREFETHEN, L. N. 2004. An extension of MATLAB to continuous functions and operators. *SIAM Journal on Scientific Computing,* 25**,** 1743-1770.

BOYD, J. P. 2001. *Chebyshev and Fourier spectral methods*, Courier Corporation.

CARPENTER, S. R. & BROCK, W. 2006. Rising variance: a leading indicator of ecological transition. *Ecology Letters,* 9**,** 311-318.

CHEBYSHEV, P. L. V. 1853. *Théorie des mécanismes connus sous le nom de parallélogrammes*, Imprimerie de l'Académie impériale des sciences.

DOROGOVTSEV, S. N., GOLTSEV, A. V. & MENDES, J. F. 2008. Critical phenomena in complex networks. *Reviews of Modern Physics,* 80**,** 1275.

DRISCOLL, T. A., HALE, N. & TREFETHEN, L. N. 2014. Chebfun guide. Pafnuty Publications, Oxford.

GAO, J., BARZEL, B. & BARABÁSI, A.-L. 2016. Universal resilience patterns in complex networks. *Nature,* 530**,** 307.

ISELLA, L., STEHLE, J., BARRAT, A., CATTUTO, C., PINTON, J. & DEN BROECK, W. V. 2011. What's in a crowd? Analysis of face-to-face behavioral networks. *Journal of Theoretical Biology,* 271**,** 166-180.

IVES, A. R. 1995. Measuring resilience in stochastic systems. *Ecological Monographs,* 65**,** 217-233.

LAURENCE, E., DOYON, N., DUBÉ, L. J. & DESROSIERS, P. 2019. Spectral dimension reduction of complex dynamical networks. *Physical Review X,* 9**,** 011042.

LYAPUNOV, A. M. 1992. The general problem of the stability of motion. *International journal of control,* 55**,** 531-534.

MASON, J. C. & HANDSCOMB, D. C. 2002. *Chebyshev polynomials*, Chapman and Hall/CRC.

PACHÓN, R. & TREFETHEN, L. N. 2009. Barycentric-Remez algorithms for best polynomial approximation in the chebfun system. *BIT Numerical Mathematics,* 49**,** 721.

PAN, L., YANG, D., WANG, W., CAI, S., ZHOU, T. & LAI, Y.-C. 2020. Phase diagrams of interacting spreading dynamics in complex networks. *Physical Review Research,* 2**,** 023233.

ROSSI, R. A. & AHMED, N. K. The Network Data Repository with Interactive Graph Analytics and Visualization. AAAI, 2015.

SCHEFFER, M., BASCOMPTE, J., BROCK, W. A., BROVKIN, V., CARPENTER, S. R., DAKOS, V., HELD, H., VAN NES, E. H., RIETKERK, M. & SUGIHARA, G. 2009. Early-warning signals for critical transitions. *Nature,* 461**,** 53.

SCHEFFER, M., CARPENTER, S. R., LENTON, T. M., BASCOMPTE, J., BROCK, W., DAKOS, V., VAN DE KOPPEL, J., VAN DE LEEMPUT, I. A., LEVIN, S. A. & VAN NES, E. H. 2012. Anticipating critical transitions. *Science,* 338**,** 344-348.

SORNETTE, D. 2006. *Critical phenomena in natural sciences: chaos, fractals, selforganization and disorder: concepts and tools*, Springer Science & Business Media.

STANLEY, H. E. 1999. Scaling, universality, and renormalization: Three pillars of modern critical phenomena. *Reviews of modern physics,* 71**,** S358.

SUWEIS, S. & D'ODORICO, P. 2014. Early warning signs in social-ecological networks. *PloS one,* 9**,** e101851.

THIBEAULT, V., ST-ONGE, G., DUBÉ, L. J. & DESROSIERS, P. 2020. Threefold way to the dimension reduction of dynamics on networks: an application to synchronization. *arXiv preprint arXiv:.10922*.

TOWNSEND, A. & TREFETHEN, L. N. 2013. An Extension of Chebfun to Two Dimensions. *SIAM Journal on Scientific Computing,* 35**,** C495-C518.

TREFETHEN, L. N. 2013. *Approximation theory and approximation practice*, Siam.

VAN NES, E. H. & SCHEFFER, M. 2007. Slow recovery from perturbations as a generic indicator of a nearby catastrophic shift. *The American Naturalist,* 169**,** 738-747.

WISSEL, C. 1984. A Universal Law of the Characteristic Return Time near Thresholds. *Oecologia,* 65**,** 101-107.